

Glial Hedgehog signalling and lipid metabolism regulate neural stem cell proliferation in *Drosophila*

Qian Dong^{1,2} , Michael Zavortink^{1,2}, Francesca Froidi^{1,2}, Sofya Golenkina^{1,2}, Tammy Lam^{1,2} & Louise Y Cheng^{1,2,3,*} 

Abstract

The final size and function of the adult central nervous system (CNS) are determined by neuronal lineages generated by neural stem cells (NSCs) in the developing brain. In *Drosophila*, NSCs called neuroblasts (NBs) reside within a specialised microenvironment called the glial niche. Here, we explore non-autonomous glial regulation of NB proliferation. We show that lipid droplets (LDs) which reside within the glial niche are closely associated with the signalling molecule Hedgehog (Hh). Under physiological conditions, cortex glial Hh is autonomously required to sustain niche chamber formation. Upon FGF-mediated cortex glial overgrowth, glial Hh non-autonomously activates Hh signalling in the NBs, which in turn disrupts NB cell cycle progression and its ability to produce neurons. Glial Hh's ability to signal to NB is further modulated by lipid storage regulator lipid storage droplet-2 (*Lsd-2*) and de novo lipogenesis gene fatty acid synthase 1 (*Fasn1*). Together, our data suggest that glial-derived Hh modified by lipid metabolism mechanisms can affect the neighbouring NB's ability to proliferate and produce neurons.

Keywords *Drosophila*; glial niche; Hedgehog; lipid metabolism; neuroblast

Subject Categories Metabolism; Neuroscience; Stem Cells & Regenerative Medicine

DOI 10.15252/embr.202052130 | Received 19 November 2020 | Revised 11 February 2021 | Accepted 12 February 2021 | Published online 10 March 2021
EMBO Reports (2021) 22: e52130

Introduction

Most stem cells reside within specialised groups of cells, collectively referred to as a niche, that provide the trophic, structural and nutritional microenvironment to sustain and protect the stem cells during development (Scadden, 2014). The niche relays developmental and physiological states of the animal to the stem cells and influences the stem cells' ability to divide in accordance with the environmental state of the organism. Asymmetrically dividing and multipotent neural stem cells in both mammals and invertebrates are responsible for generating the adult nervous system (Homem & Knoblich, 2012).

In *Drosophila*, the vast majority of NBs are specified during embryogenesis, proliferate throughout larval development and terminate divisions during pupal stages. Type I NBs located within the ventral nerve cord (VNC) and the central brain (CB) are the predominant type of NBs, whilst type II NBs are eight NB lineages located on the dorsal surface of the CB (Homem & Knoblich, 2012). During each type I NB cell division, NB self-renews and produces a smaller ganglion mother cell (GMC) that creates a limited number of neurons or glia (Fig 1A). The ability of NBs to divide and generate appropriate progeny number and cell diversity is determined by their ability to maintain asymmetric division, regulate the speed of their cell cycles and timely enter/exit the cell cycle at the beginning and end of neurogenesis (Homem & Knoblich, 2012). Cell intrinsic mechanisms such as the temporal regulation of NB identity via transcription factors that are expressed throughout the life time of the NBs impact on both the numbers and the types of neurons generated by the NB (Doe, 2017). However, more recently, attention has shifted towards understanding how cell extrinsic signals are interpreted by the NBs to alter their behaviour (Ramon-Canellas *et al*, 2019).

Larval NBs and their progeny are surrounded by a scaffold of glial cell processes, which form the stem cell niche in the CNS (Fig 1A). Glial cells fall into three classes: (i) surface (perineural and subperineural) glia that enwrap the CNS to form the blood brain barrier (BBB); (ii) cortex glia that encapsulate neuronal soma and NBs; and (iii) neuropil glia that are located at the cortex–neuropil interface and form a sheath around the neuropil compartments (Freeman, 2015).

The intimate relationship between glial cells and NBs has been extensively studied in the context of NB entry into the cell cycle at the beginning of post-embryonic neurogenesis shortly after larval hatch (Ding *et al*, 2020). Feeding has been shown to trigger insulin production by surface glial cells, which in turn activates the insulin/insulin-like growth factor pathway in neighbouring NBs and stimulates their growth and proliferation via activation of the phosphoinositide 3-kinase (PI3K) signalling pathway (Chell & Brand, 2010; Sousa-Nunes *et al*, 2011). Once NBs enter into the cell cycle, glial cells continue to play active roles in promoting NB proliferation. These reactivated NBs are found in close association with cortex glia (Hoyle, 1986; Hoyle *et al*, 1986; Peraanu *et al*, 2005), and this contact is maintained through adhesion via E-cadherin. Disruption

1 Peter MacCallum Cancer Centre, Parkville, Vic., Australia

2 Sir Peter MacCallum Department of Oncology, University of Melbourne, Parkville, Vic., Australia

3 The Department of Anatomy and Neuroscience, University of Melbourne, Parkville, Vic., Australia

*Corresponding author. Tel: +61 450053363; E-mail: louise.cheng@petermac.org

of NB-cortex glia contact affects the NB's ability to undergo mitosis (Dumstrei *et al*, 2003; Doyle *et al*, 2017), and the failure to expand the glial membrane also affects both neuronal survival as well as NB cell cycle progression (Speder & Brand, 2018; Yuan *et al*, 2020). Diffusible molecules that pass from glial cells to influence NB behaviour include Dally-like (Dlp) in the perineural glia, (Kanai *et al*, 2018) and Jellybelly (Jeb) in the cortex glia (Cheng *et al*, 2011). Furthermore, organelles such as lipid droplets (LDs) in the glial niche have been shown to buffer NBs proliferation from

peroxidation chain reactions induced by oxidative stress (Bailey *et al*, 2015), suggesting that glial niche and the signalling molecules produced by these cells are important mediators of non-autonomous regulation of NB behaviour during developmental and environmental stress.

In this study, we investigate how the stem cell niche and its dysfunction influence stem cell behaviour and the consequences on the brain as a whole. We found that the signalling molecule Hedgehog (Hh), involved in numerous developmental processes, resides

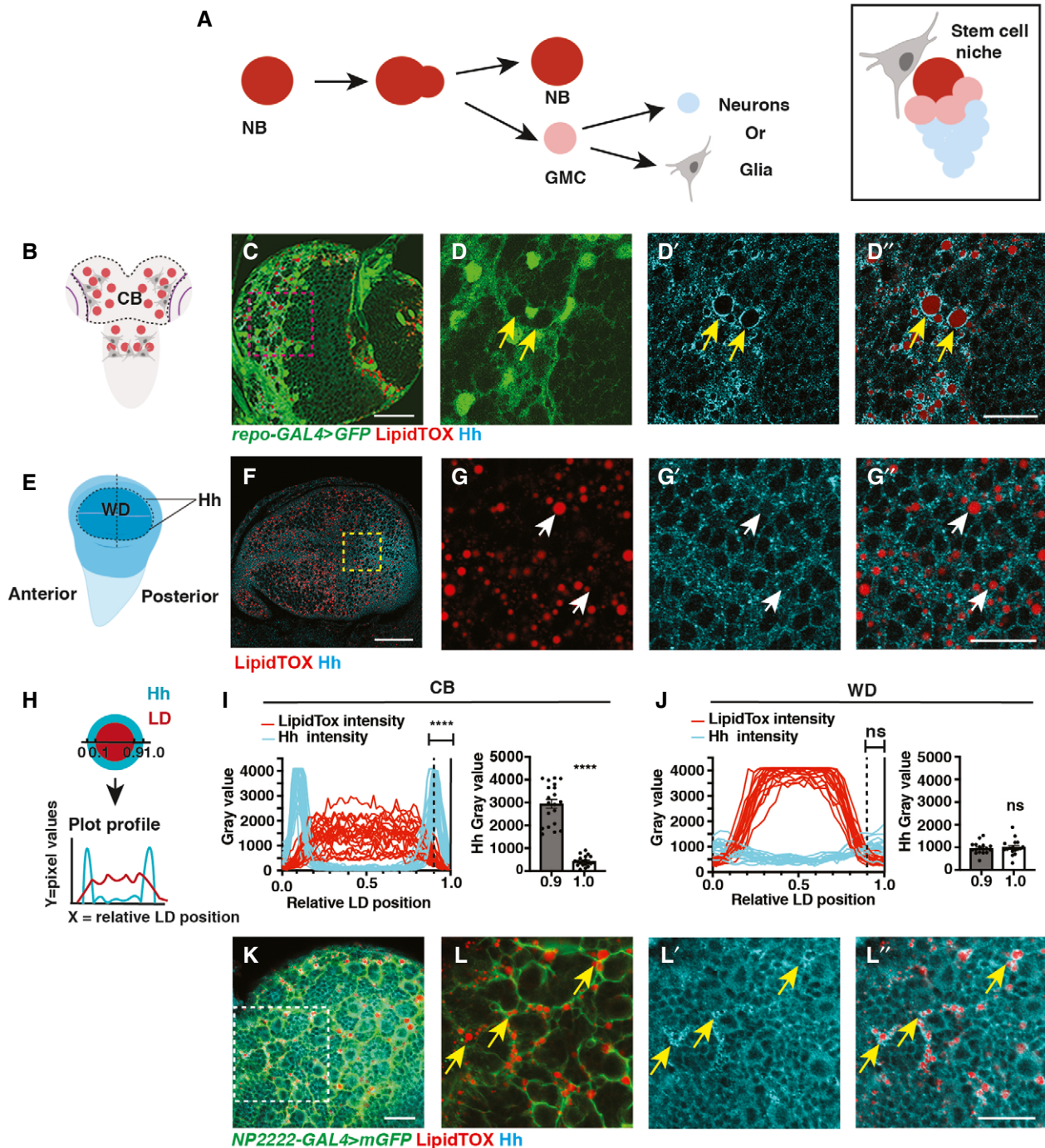


Figure 1.

Figure 1. Hh is localised to the LDs within cortex glial cells.

Images in this and following figures are of larval central brains (CBs) at 96ALH.

- A Schematic showing NBs that undergo asymmetric division to self-renew and produce GMCs, which terminally differentiate to generate post-mitotic neurons or glial cells (left). Each NB is surrounded by a microenvironment, composed of glial cells (right).
- B–D” Representative images showing that Hh accumulates on the surface of LDs in glial cells of the CB (yellow arrows), quantified in (I) ($n = 20$ LDs). Glial cells are marked by *repo-GAL4 > GFP* and CB is circled in (B).
- E–G” In the posterior compartment of the developing wing disc (WD) pouch region where Hh is expressed, LDs and Hh are not tightly associated (white arrows), quantified in (J) ($n = 17$ LDs).
- H–J Hh-LD association is quantified by plotting the pixel intensities of both Hh (cyan) and LDs (red) along a line across LDs. Y-axis represents grey intensity values, and X-axis represents relative LD position.
- K, L” Hh-LD associations are observed in the cortex glia (yellow arrows, *NP2222-GAL4 > mGFP*).

Data information: Hh is detected with a Hh antibody and LDs are visualised with LipidTOX unless otherwise stated. (D–D”), (G–G”), (L–L”) are zoomed in images of (C, F, K), respectively. Scale bar = 50 μm in (C and F), scale bar = 20 μm in (D–D”, K–L”), scale bar = 10 μm in (G–G”). Error bar represents SEM. In (I): Welch’s *t*-test, (****)

$P < 0.0001$. In (J): unpaired *t*-test, (ns) $P = 0.7113$.

Source data are available online for this figure.

within the cortex glial membrane that surrounds NBs. Hh is autonomously required to promote glial niche growth as well as acts non-cell autonomously to activate the Hh signalling in the NB, triggering its delay in S phase progression. Maintaining cortex glial size is important, as overgrowth induced by FGF activation, a mutation implicated in glioblastoma (Morrison *et al*, 1994; Yamada *et al*, 1999; Dienstmann *et al*, 2014; Jimenez-Pascual & Siebzehnrubl, 2019), phenocopied the effects of glial Hh activation on NBs. Indeed, inhibiting Hh rescued NB proliferation defects. Furthermore, we demonstrated that downstream of glial FGF signalling, Hh activity and its ability to signal to NBs are modulated by two lipid storage regulators *Lsd-2* and *Fasn1*. Together, our data show that a dysfunctional niche can non-autonomously affect NB’s ability to produce the correct number of neurons that make up the adult CNS. This process mechanistically involves the Hh signalling pathway and its modulation by lipid metabolism.

Results

Hh is localised to the LDs within cortex glial cells

To identify potential morphogens that facilitate glia-NB communication in the CB, we assayed for secreted molecules which are known to act in a paracrine fashion. We found that Hh is expressed at high levels at 96 h After Larval Hatching (96ALH) in glial cells labelled using *Repo-GAL4 > GFP* (Fig 1B–D”). Hh is a morphogen that was first identified to regulate embryo segmentation and wing imaginal disc development (Nusslein-Volhard & Wieschaus, 1980; Heemskerck & DiNardo, 1994). In the wing disc, it is expressed in the posterior compartment and is distributed in a gradient to regulate target gene expression in the anterior compartment (Fig 1E and F) (Chen *et al*, 2017). In the glial niche, however, we found Hh staining was mostly distributed in ring-like structures in the glial cytoplasm (yellow arrows, Fig 1C and D”). We then assessed whether Hh is associated with specific organelles. LDs are round-shaped organelles, consisting of a hydrophobic core for the storage of neutral lipids and a phospholipid monolayer containing LD surface proteins. As LDs have previously been reported to be enriched in the glial niche (Bailey *et al*, 2015; Kis *et al*, 2015), we therefore tested whether Hh ligands are associated with LDs. Using a neutral lipid stain, lipidTOX to visualise LDs and either an antibody, or a BAC encoded Hh:GFP

to detect Hh (Chen *et al*, 2017), we found that Hh is localised to the surface of the LDs in the glial niche (yellow arrows, Figs 1C and D”, I, and EV1A and B”), but not in the wing disc (white arrows, Figs 1F and G”, J, and Fig EV1C–D”) nor at earlier stages of development in the CB (48 ALH, Fig EV2A and B”). Together, our data suggest that Hh is localised to the surface of LDs in the glial niche.

We next explored whether Hh-LD associations are specifically localised to a glial subtype. Hh-LD associations were largely absent from both surface glial cells that forms the blood brain barrier (BBB) of the CNS (white arrows, Fig EV2E and F”), as well as optic lobe glial cells (white arrows, Fig EV2C and D”). In fact, Hh-LD associations were enriched in the cortex glial cells, underneath the sheath-like surface glial clone generated via *repo-MARCM* (yellow arrows, Fig EV2G). Using a cortex-specific driver, *NP2222-GAL4* (Hayashi *et al*, 2002; Awasaki *et al*, 2008), we confirmed that the Hh-LD associations were localised to the cortex glia (Fig 1K and L”).

Hh autonomously regulates cortex gliogenesis and non-autonomously regulates NB proliferation

In the mouse brain, Hh has been shown to promote astrocyte proliferation (Takezaki *et al*, 2011; Chandra *et al*, 2015; Ugboode *et al*, 2017). In glioblastoma (GBM), the Hh/Gli1 signalling pathway acts to accelerate cell proliferation (Chandra *et al*, 2015). To investigate the role of Hh in *Drosophila* cortex glial cells, where Hh is most abundant, we used pan-glial driver *repo-GAL4* to express *hh* RNAi together with *UAS-Dcr2* (*Dicer-2*) which sufficiently depleted Hh expression and reduced overall CNS size (Fig EV3A–D). The reduction in CNS volume was accounted for by a significant decrease in *Repo*⁺ glial cell number and membrane size (labelled using *NP2222-GAL4 > GFP*, Fig 2A–D). Using a pan-glial driver *repo-GAL4*, we found cortex glial chambers were significantly disrupted upon Hh knockdown (Speder & Brand, 2018; Yuan *et al*, 2020), leading to clustering of NBs (compare Fig 2G to F). However, overexpression of Hh did not affect glial cell number nor membrane size (Fig EV3L–O). This suggests Hh is necessary but not sufficient for glial expansion during CNS development.

Given the role of Hh as a secreted ligand that can act over short range within the NB lineage (Chai *et al*, 2013) and that it is highly expressed in the cortex glial niche surrounding NBs, it is plausible that glial Hh non-autonomously affects NB proliferation. We next explored the potential impact of glial Hh on the activities of type I

NBs. As Hh is required to maintain the glial niche (Fig 2A–D, F and G) and niche impairment has been shown to induce NB elimination (Read, 2018), we first assessed for alterations in NB number. We found that pan-glial Hh knockdown (*repo-GAL4*) did not significantly alter NB number (Fig EV3G), suggesting that NB survival is unaffected. We then investigated the effects of glial Hh knockdown on NB proliferation. Glial Hh knockdown using *repo-GAL4* induced a small increase in the percentage of NBs in M phase (pH3 index;

Fig 2E). To assess NB S phase progression, we examined EdU (5-ethynyl-2'-deoxyuridine) incorporation during a 15-min time window (EdU index, Fig EV3E, yellow arrows). Here, we found EdU incorporation was significantly reduced upon glial Hh knockdown, suggesting that fewer NBs entered into the S phase of the cell cycle (Fig EV3F). Interestingly, a similar alteration of NB pH3 and EdU index was observed upon glial niche impairment caused by PI3K signalling inhibition (Speder & Brand, 2018). Therefore, it is likely

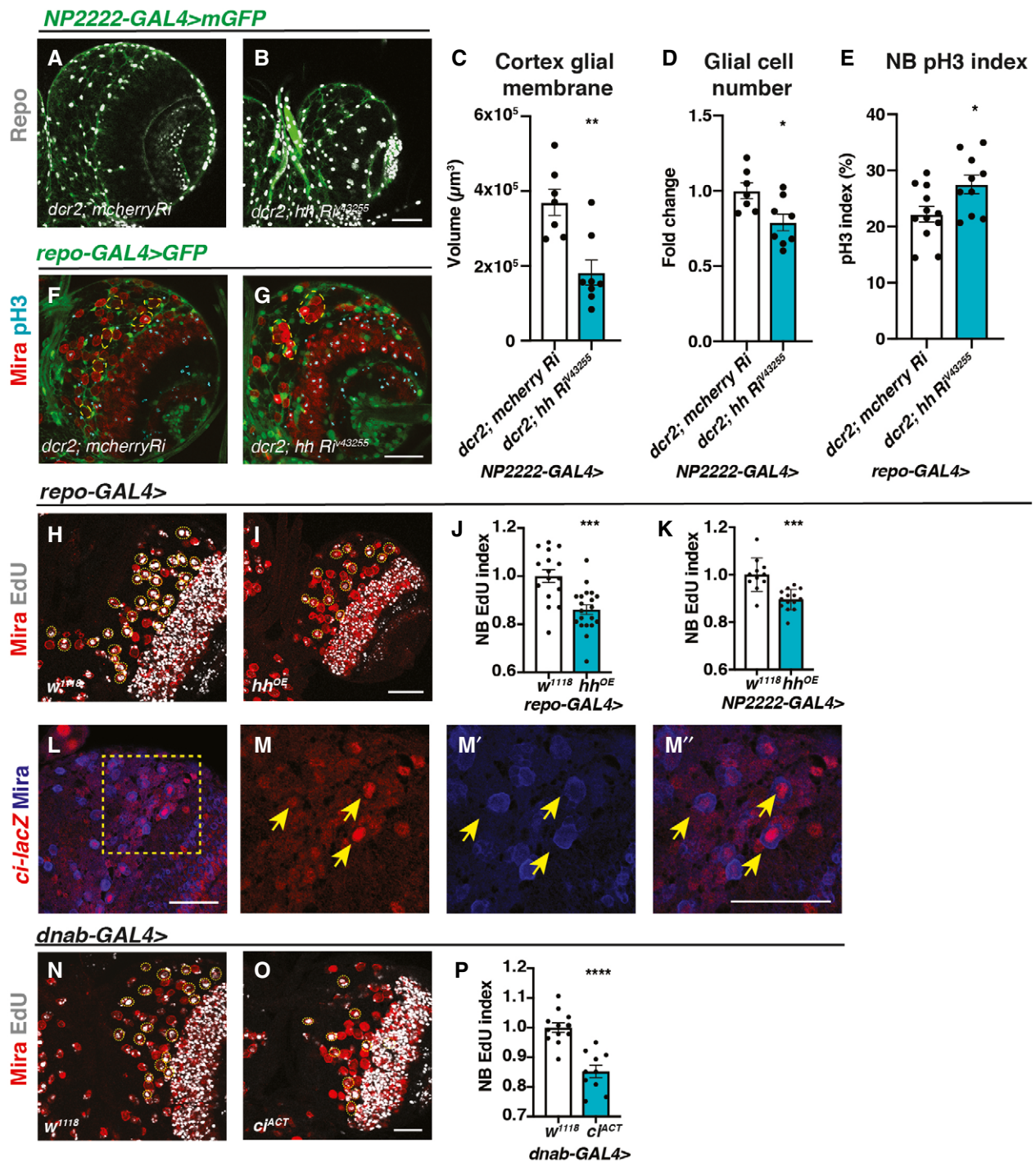


Figure 2.

Figure 2. Hh autonomously regulates cortex gliogenesis and non-autonomously regulates NB proliferation.

A–D Representative images showing that upon knockdown of Hh in cortex glial cells (*NP2222-GAL4 > mGFP with UAS-dcr2*), cortex glial membrane and overall Repo + glial cell number are significantly reduced, quantified in (C) ($n = 7, 8$ brain lobes) and (D) ($n = 7, 8$ brain lobes), respectively.

E–G Hh knockdown in glia (*repo-GAL4 > GFP*) results in niche disruption and clustering of NBs (circled with yellow dashed line), as well as an increase in the percentage of NBs in M phase (pH3⁺), quantified in (E) ($n = 12, 10$ brain lobes).

H–K Representative images showing that Hh overexpression using pan-glial (*repo-GAL4*) and cortex glial (*NP2222-GAL4*) drivers both result in a decrease in NB EdU index, quantified in (J) ($n = 16, 20$ brain lobes) and (K) ($n = 11, 14$ brain lobes), respectively.

L–M^{''} Representative images showing *ci-lacZ* is expressed in NBs (yellow arrows). (M–M^{''}) are zoomed in images of (L).

N–P Overexpression of *ci^{ACT}* in NBs (*dnab-GAL4*) reduces EdU index, quantified in (P) ($n = 12, 10$ brain lobes).

Data information: NBs are marked with Mira and EdU⁺ NBs are circled by yellow dashed line. Scale bar = 50 μ m. Error bar represents SEM. In (C): Mann–Whitney test, (***) $P = 0.0059$. In (D): unpaired *t*-test, (*) $P = 0.0176$. In (E): unpaired *t*-test, (*) $P = 0.0215$. In (J): unpaired *t*-test, (***) $P = 0.0002$. In (K): unpaired *t*-test, (***) $P = 0.0001$. In (P): unpaired *t*-test, (****) $P < 0.0001$.

Source data are available online for this figure.

that glial Hh depletion indirectly causes NBs to stall at M phase via inhibition of cortex glial chamber formation. To investigate the effect of glial Hh depletion on NB progeny production, we conducted EdU pulse-chase assay, where larvae were fed food supplemented with EdU for 3 h and chased for 3 h in EdU-free food (Fig EV3H). Using *pros:GFP* which marks individual NB lineages, we found the number of GFP⁺ and EdU⁺ cells per lineage was significantly reduced upon cortex glial Hh knockdown (Fig EV3I–K). Together, these results suggest that NB proliferation is inhibited upon cortex glial niche impairment caused by Hh knockdown.

The subperineural glial Dlp and the cortex glial Jeb promote NB proliferation during development; however, overexpression of these signalling molecules in the glial niche was not sufficient to increase NB cell cycle rate (Cheng *et al*, 2011; Kanai *et al*, 2018). We next assessed the effect of glial Hh overexpression on NB behaviour. Pan-glial induction of Hh did not significantly alter NB number (Fig EV3G). However, pan-glial and cortex glial-specific Hh overexpression caused a reduction in NB EdU incorporation (Fig 2H–K). Using reporter lines of Hh activity *ci-lacZ* (Schwartz *et al*, 1995) and Ptc:mCherry (Varjosalo & Taipale, 2008; Chen *et al*, 2017), we found that Hh signalling is highly active in the NBs (Figs 2L and M^{''} and EV3P and Q^{''}), consistent with a previous report by (Chai *et al*, 2013). Furthermore, activation of Hh transcriptional activator *cubitus interruptus* (*ci^{Nc5m5m}* or *ci^{ACT}*) with a NB-specific driver *dnab-GAL4* (Maurange *et al*, 2008) significantly reduced NB EdU index (Fig 2N–P), phenocopying the effects of glial Hh overexpression. Together, our data suggest that high levels of glial Hh expression restrict NB cell cycle progression.

Hh activity is modulated by Lsd-2

Lipid storage droplet-2 (*Lsd-2*) is the *Drosophila* orthologue of the mammalian perilipin2 and a widely used marker of LDs (Teixeira *et al*, 2003) (Fig 3A and B^{''}). Using a GFP reporter against *Lsd-2* together with Hh antibody, we observed that *Lsd-2* and Hh colocalise to the surface of LDs in the cortex glia (yellow arrows, Fig 3C and D^{''}). To explore whether *Lsd-2* affects Hh activity, we knocked down *Lsd-2* whilst overexpressing Hh in cortex glial cells (*NP2222-GAL4 >*). *Lsd-2* is known to block the access of lipases, thus promoting lipid storage (Teixeira *et al*, 2003). As expected, knockdown of *Lsd-2* caused a significant reduction in LDs (Fig 3E–G). Furthermore, this also significantly rescued the NB EdU incorporation defects caused by *hh* overexpression (Fig 3H–K), suggesting *Lsd-2* modulates Hh's ability to signal to NBs.

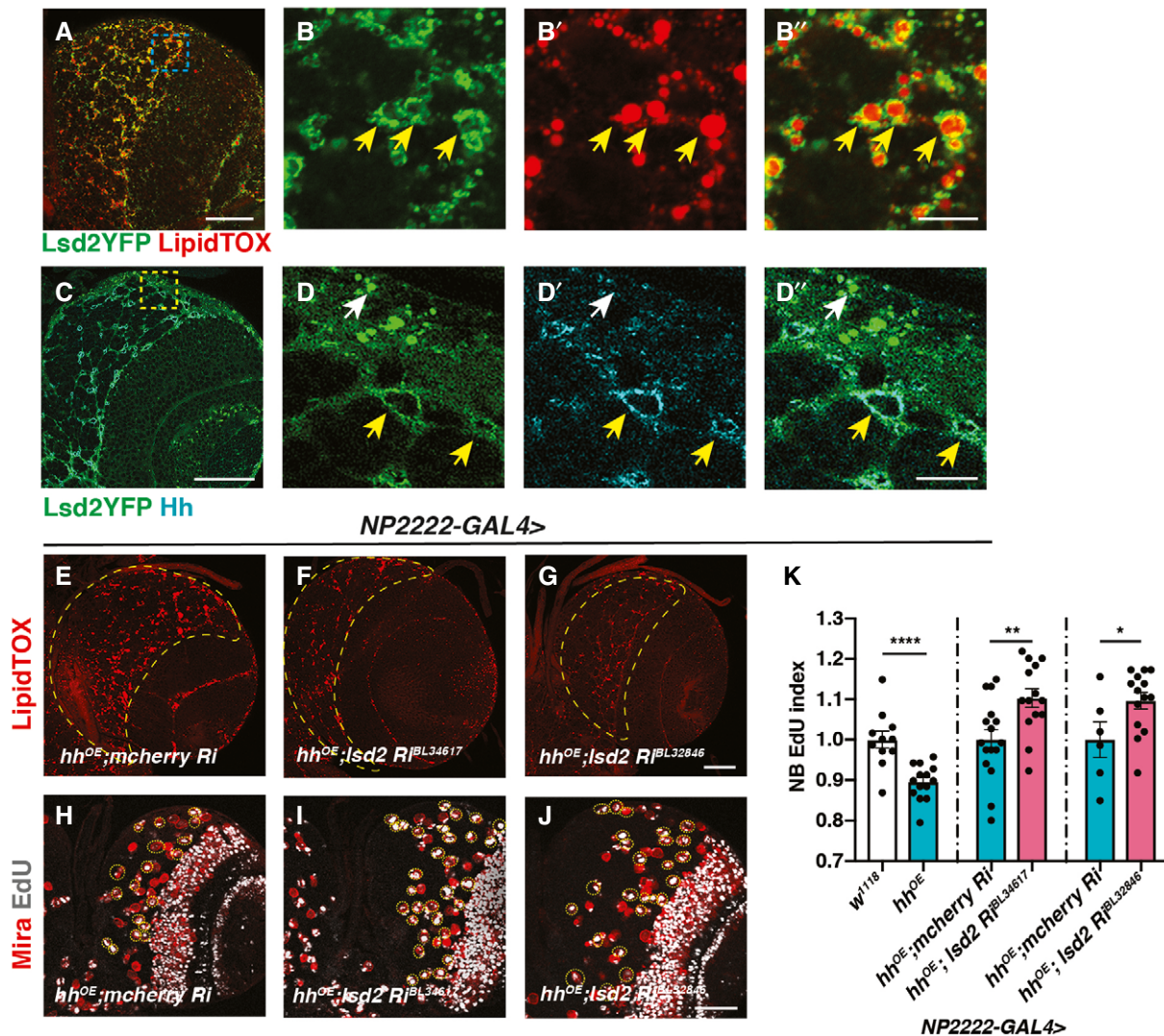
FGFR, but not EGFR or InR, activation induces cortex glial overgrowth

Given that we found Hh activity is modulated by a lipid modulator *Lsd-2*, it is possible that Hh might act in disease contexts such as glioblastoma, where glial cells undergo increased proliferation and lipid metabolism alterations (Geng & Guo, 2017). As Hh/LD associations mostly localised to the cortex glia that enwrap NBs, we explored the role for cortex glial overgrowth, using previously characterised glioma models, involving the activation of FGF, InR and EGFR (Read *et al*, 2009; Witte *et al*, 2009; Reddy & Irvine, 2011; Avet-Rochex *et al*, 2012). Firstly, we characterised the effect of overexpression of a wild-type form of InR, constitutively activated form of the FGF receptor Heartless (*Htl*) and EGFR. Consistent with the observation of (Avet-Rochex *et al*, 2012), we found *htl^{ACT}* but not *InR^{wt}* overexpression caused an expansion of the cortex glial niche which enwraps NBs (Fig 4A–C, A'–C'). In contrast, *Egfr^{ACT}* overexpression, which acts through Ras signalling, did not affect cortex glial niche size (Fig 4A and A', D and D'). Using cortex glial-specific *NP2222-GAL4* and *wrapper-GAL4* (Coutinho-Budd *et al*, 2017; Richier *et al*, 2017), we found that cortex glial overexpression of *htl^{ACT}*, but not *InR^{wt}* or *Egfr^{ACT}*, led to an increase in total glial cell numbers (Fig 4E–G, I–K). Finally, *htl^{ACT}* overexpression significantly increased the size of the cortex glial membrane (Fig 4E and F, H). Together, our data suggest the activation of FGF, but not InR or EGFR, induced cortex glial niche overgrowth.

We next explored the impact of glial niche overgrowth on NBs. Using the pan-glial driver *repo-GAL4*, we measured NB cell number and its impact on the cell cycle assessed with pH3 index. We found that *InR^{wt}*, but not *htl^{ACT}* and *Egfr^{ACT}* overexpression, caused a reduction in NB number, reminiscent of the NB elimination phenotype reported for glial *Pvr^{ACT}* overexpression (Read, 2018) (Fig 4L). In addition, only overexpression of *htl^{ACT}*, which induced cortex glial overgrowth, caused a reduction of NB pH3 index, whilst *InR^{wt}* and *Egfr^{ACT}* overexpression did not significantly alter NB cell cycle progression (Fig 4M). Together, these data indicate that cortex glial niche is the key glial subset that mediates glia–NB crosstalk, and its expansion driven by FGF activation affected NB cell cycle progression.

Cortex glial overgrowth mediated by FGF activation slows down NB cell cycle progression

To further investigate the effect of glial FGF activation on NB cell cycle, we assessed S phase progression via EdU incorporation. FGF



activation using pan-glial (*repo-GAL4*) as well as cortex glial (*NP2222-GAL4*) drivers caused a significant reduction in NB EdU index (Fig 5A–E). Consistent with the reduction in pH3 index (Fig 4M), these experiments confirm that the cortex glia is responsible for NB cell cycle delay induced by FGF activation.

We next examined the cell cycle length of NBs using live cell imaging on explanted brains, where three brains containing multiple NBs labelled with Dpn::GFP and His::RFP (Fig 5G and H) were imaged. We found FGF activation with *repo-GAL4* induced a severe slowing down of the cell cycle at 96ALH, such that we could not

capture any entire NB cell cycles within an 8-h time window. Previously, it was reported that NBs cycle faster during earlier developmental stages (Maurange *et al*, 2008; Chai *et al*, 2013), and therefore, we imaged NB divisions at 72 ALH. We observed that glial FGF activation lengthened NB cell cycle from 100.2 ± 6.0 min to 250.0 ± 28.4 min (Fig 5F, Movies EV1 and EV2).

To decipher which phase of the cell cycle was affected, we generated flies expressing *htl^{ACT}* downstream of a *LexA* operator (*LexAop*) (Lai & Lee, 2006). Overexpressing *htl^{ACT}* using *repo-LexA/LexAop* system enabled us to concurrently induce NB-specific

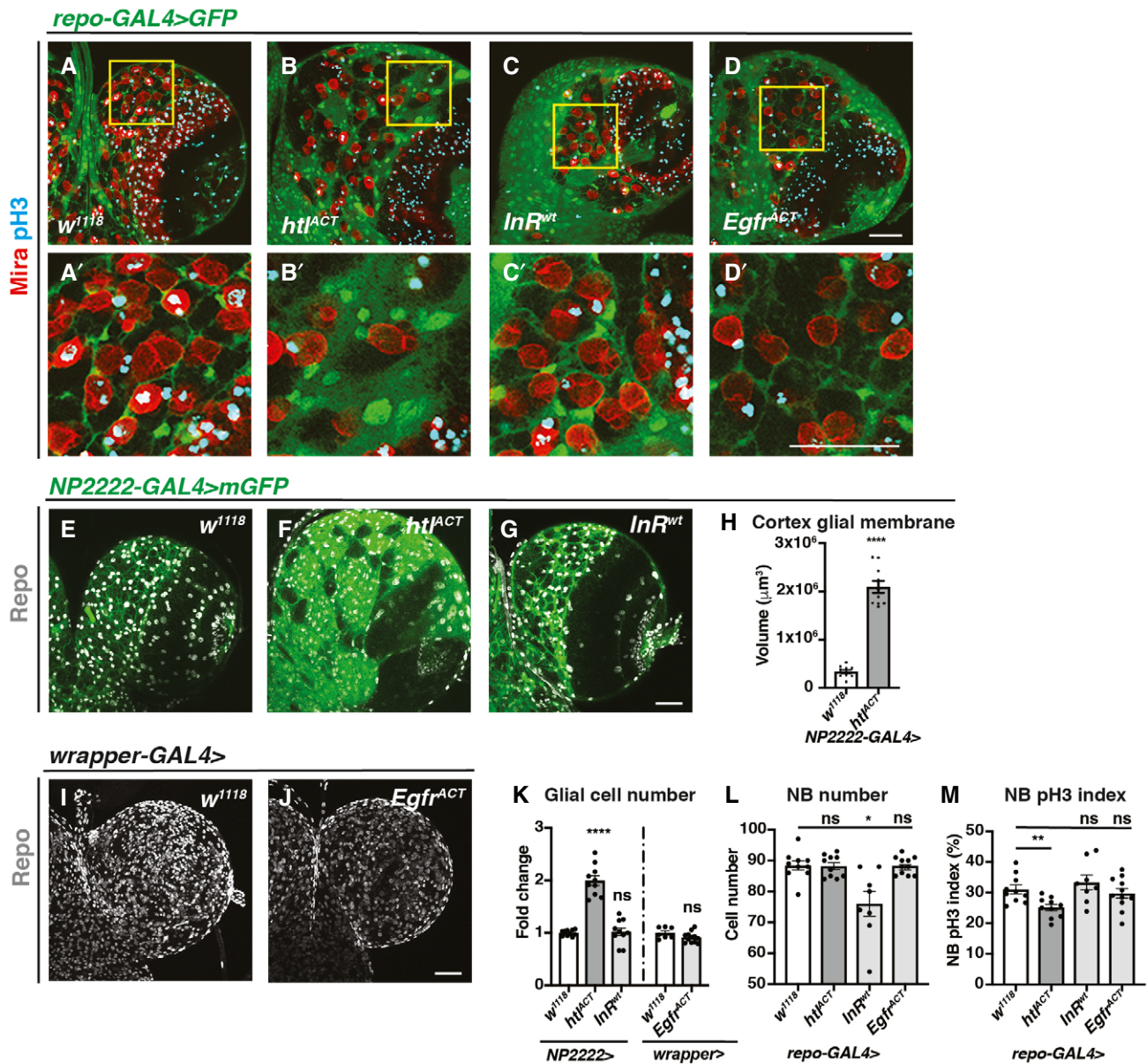


Figure 4. Activation of *ht^{ACT}* but not *InR^{wt}* and *Egfr^{ACT}* induces cortex glial overgrowth.

A–D' Representative images showing that pan-glial overexpression of *ht^{ACT}*, but not *InR^{wt}* or *Egfr^{ACT}* causes an expansion of cortex glia that enwraps NBs. Glial cells are marked with *repo-GAL4 > GFP*, and NBs are marked with Mira. (A', B', C' and D') are zoomed in images of (A, B, C and D), respectively.

E–K Representative images showing that cortex glial overexpression of *ht^{ACT}* but not *InR^{wt}* or *Egfr^{ACT}* causes an increase in glial cell (*Repo⁺*) numbers and cortex glial membrane size, quantified in (K) ($n = 10, 10, 10; 7, 12$ brain lobes) and (H) ($n = 10, 10$ brain lobes), respectively. *NP2222-GAL4 > mGFP* is used to mark cortex glial membrane in (E–G) and *wrapper-GAL4 >* is used in (I, J).

L Glial (*repo-GAL4>*) overexpression of *InR^{wt}* but not *ht^{ACT}* or *Egfr^{ACT}* significantly reduces the number of CB NBs ($n = 10, 10, 8, 11$ brain lobes).

M Glial (*repo-GAL4>*) overexpression of *ht^{ACT}* but not *InR^{wt}* or *Egfr^{ACT}* significantly reduces the p3H index of CB NBs (marked with Mira and p3H in (A–D')) ($n = 10, 10, 8, 11$ brain lobes).

Data information: Scale bar = 50 μm . Error bar represents SEM. In (H): Welch's *t*-test, (****) $P < 0.0001$. In (K): Welch's *t*-test, (****) $P < 0.0001$; Welch's *t*-test, (ns) $P = 0.7905$; unpaired *t*-test, (ns) $P = 0.0941$. In (L): unpaired *t*-test, (ns) $P = 0.9140$; Welch's *t*-test, (*) $P = 0.0170$; unpaired *t*-test, (ns) $P = 0.9825$. In (M): unpaired *t*-test, (**) $P = 0.0038$; unpaired *t*-test, (ns) $P = 0.4172$; unpaired *t*-test, (ns) $P = 0.5523$.

Source data are available online for this figure.

expression of Fly-Fucci using *dnab-GAL4* (as depicted in Fig 5I schematic). With Fly-Fucci, cell cycle phases can be identified using combinations of two fluorescent fusion proteins (Zielke et al, 2014).

Surprisingly, we found glial FGF activation significantly increased the percentage of NBs in G2/M and G1-S transition at the expense of cells in G1 phase (Fig 5J–L). As the percentage of NBs in M phase

(reflected by pH3 index) was reduced upon glial FGF activation, we conclude that these NBs are potentially stalled at G2/ G2-M and G1-S transitions of the cell cycle. As a result, NBs cannot efficiently enter S phase or M phase, as indicated by reduced EdU and pH3 indices (Fig 5A–E, and 4M), and, therefore, undergo a dramatically lengthened cell cycle (Fig 5F).

We expect that slowing down of the NB cell cycle upon glial FGF activation would consequentially affect the number of neurons generated by NBs. To test this hypothesis, we conducted EdU pulse-chase assay (3-h feeding followed by a 4-h chase) and counted the number of EdU⁺ neurons per lineage, which are marked by *dnab-GAL4::UAS-GFP*. We found that overexpression of *htl^{ACT}* with *repo-LexA/LexAop* significantly reduced the number of EdU⁺ neurons

generated per NB (Fig 5M–O). Together, our data indicate that FGF activation in cortex glial cells prevents NB cell cycle progression and its ability to produce the correct number of neurons.

Glial FGF activation affects NB asymmetric division, size and cell cycle exit

Given that cell polarity that contributes to NB asymmetric division is established in the G2/M phase, we then assessed whether NB asymmetric division is affected upon glial FGF activation. In the wild type, inscuteable, an adaptor protein that connects the aPKC/Par3/Par6 complex to the PINS/MUD/Gai complex, forms a crescent at the apical side during NB mitosis (Doe, 1996); these apical

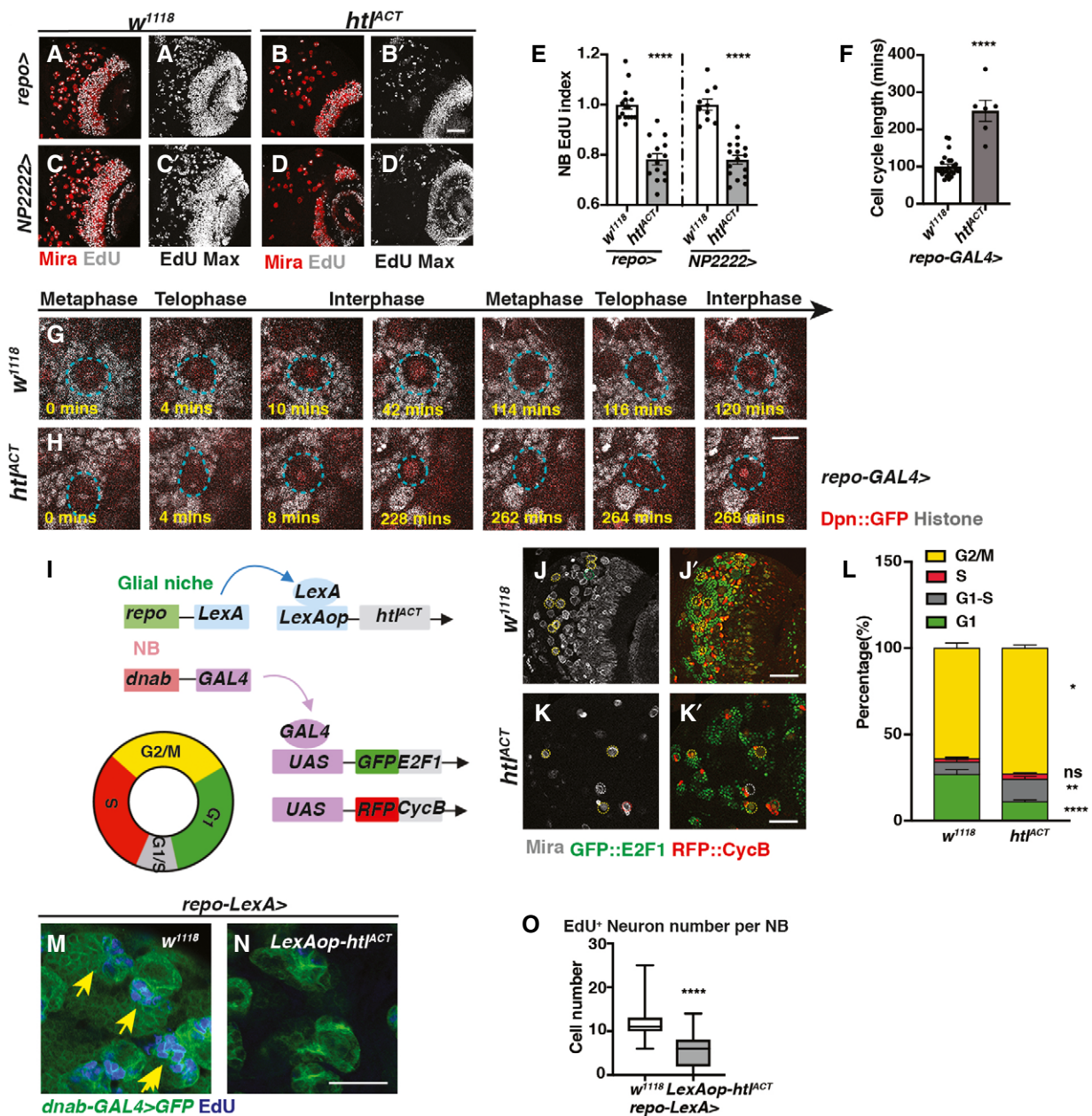


Figure 5.

Figure 5. Cortex glial overgrowth mediated by *htl^{ACT}* overexpression triggers NB cell cycle delay.

A–E Representative images showing that both pan-glial (*repo-GAL4*) and cortex glial (*NP2222-GAL4*) *htl^{ACT}* overexpression significantly reduce NB EdU index, quantified in (E) ($n = 15, 14; 10, 16$ brain lobes). (A, B, C, D) are single sections with Mira and EdU staining, and (A', B' C', D') are Z-projection of the EdU staining.

F–H Representative still images from ex vivo CNS live imaging at 72ALH showing that pan-glial (*repo-GAL4*) *htl^{ACT}* overexpression lengthens NB cell cycle, quantified in (F) ($n = 25, 6$ NBs imaged from three brains per genotype). The cell cycle length is measured as the length between consecutive divisions. NBs (Dpn::GFP, red; Histone RFP, grey) are circled with blue dashed lines.

I Schematic depicting concurrent glial FGF activation (*repo-LexA > LexAop-htl^{ACT}*), and NB overexpression of fly-FUCCI (*dnab-GAL4 > UAS-GFP::E2F1, UAS-RFP::CycB*). The fly-FUCCI system utilises the fusion protein GFP::E2F1 (a marker for cells in G2, M and G1 phase) and RFP::CycB (a marker for cells in S, G2, M phase) to monitor cell cycle progression. Cells in G1 phase are GFP⁺ RFP⁻ (green), cells in G2/ M phase are GFP⁺ RFP⁺ (yellow), and cells in S phase are GFP⁻ RFP⁺ (red), whereas cells in G1-S transition are weakly labelled by both GFP and RFP (grey).

J–L Representative images showing that the percentage of NBs in G1-S transition and G2/M phase are both significantly increased with significantly less cells remaining in G1 phase, quantified in (L) ($n = 9, 10$ brain lobes). NBs in G1 phase (Mira⁺, GFP⁺) are circled by green dashed lines; NBs in G1-S transition (Mira⁺, GFP⁺RFP⁺) are circled by grey dashed lines; NBs in S phase (Mira⁺, RFP⁺) are circled by red dashed lines, and NBs in G2/M phase (Mira⁺, GFP⁺RFP⁺) are circled by yellow dashed lines.

M–O Representative images showing that the number of EdU⁺ neurons generated per NB is significantly reduced upon pan-glial overexpression of FGF (*repo-LexA > LexAop-htl^{ACT}*; yellow arrows), quantified in (O) (Box plot, the boxes extend from the 25th to 75th percentiles; the median is marked by a central band inside the box; and the whiskers go down to the minimum value and up to the maximum value. $n = 94, 127$ NB lineages imaged from five and seven brain lobes, respectively). NB lineages are marked with *dnab-gal4 > GFP*.

Data information: Scale bar = 50 μ m in (A–D', J–K); Scale bar = 10 μ m in (G, H); Scale bar = 20 μ m in (M, N). Error bar represents SEM unless otherwise stated. In (E): unpaired *t*-test, (****) $P < 0.0001$; unpaired *t*-test, (****) $P < 0.0001$. In (F): Mann–Whitney test, (****) $P < 0.0001$. In (L): G1: Mann–Whitney test, (****) $P < 0.0001$; G1-S: unpaired *t*-test, (**) $P = 0.0064$; S: unpaired *t*-test, (ns) $P = 0.1757$; G2/M: unpaired *t*-test, (*) $P = 0.0171$. In (O): Mann–Whitney test, (****) $P < 0.0001$. Source data are available online for this figure.

complexes further direct the localisation of cell fate determinants (Brat/Pros/Numb) and their adaptor proteins Mira (Shen *et al.*, 1997) and PON to the basal cortex (as depicted in Fig EV4A). The correct distribution of polarity proteins ensures the generation of a larger daughter NB and a smaller GMC upon asymmetric division (Fig EV4H). We found mitotic NBs displayed cytoplasmic or cortical localisation of Mira and Insc upon glial FGF activation (Fig EV4B–G). Furthermore, telophase NBs and GMCs were also found to be more similar in size (evaluated as NB /GMC size ratio in Fig EV4I–K). Intriguingly, both NB and its daughter cells were larger than their wild-type counterparts, and consistent with this, the average size of mitotic NBs was also significantly larger upon glial *htl^{ACT}* overexpression (Fig EV4L, from $12.44 \pm 0.16 \mu\text{m}$ to $15.55 \pm 0.34 \mu\text{m}$). This increase in cell size was coupled with elevated cellular growth, as indicated by an increase in nucleoli size (Fig EV4M–O, from $1.28 \pm 0.05 \mu\text{m}$ to $1.61 \pm 0.05 \mu\text{m}$). It is therefore likely that the delay between consecutive cell cycles allowed these NBs to grow larger.

To investigate when glial FGF starts to impact on NB proliferation, we assessed NB EdU index at 26ALH, a time point when most NBs reactivate from quiescence, and commence post-embryonic neurogenesis (Fig EV4P). We found glial *htl^{ACT}* overexpression did not significantly affect NB EdU incorporation during a 1-h EdU pulse (Fig EV4Q–S), suggesting that glial FGF does not affect NB reactivation at the beginning of neurogenesis. We then examined whether NB termination at 24 h after pupal formation (24APF) is altered (Fig EV4T). Glial *htl^{ACT}* overexpression resulted in the presence of increased number of NBs at 24APF (Fig EV4U–W), suggesting NB cell cycle exit is possibly delayed. However, it is not clear whether NBs that persist are capable of dividing. Together, we conclude glial FGF mostly exerts its effects on reducing NB cell proliferation during late larval neurogenesis, coinciding with the time when Hh-LD associations become highly enriched in the cortex glia. Taken together, our results revealed that NB activities including its proliferation, asymmetric division and termination are affected by cortex glial niche overgrowth driven by FGF activation.

Hh mediates the effects of glial FGF signalling on NB proliferation

Given that glial Hh overexpression or activation of the Hh signalling cascade in NBs similarly inhibits NB proliferation and induces polarity protein delocalisation (Chai *et al.*, 2013); it is therefore plausible that Hh lies downstream of glial FGF to regulate NB activity. To test this hypothesis, we first assessed whether niche-derived signals including Hh and its modulators such as LD synthesis enzymes were altered. By RT-qPCR, we found *hh* mRNA was upregulated by 8-fold (normalised to *rpl32*) upon glial FGF activation (*repo-GAL4*, Fig 6A). Amongst genes that promote LD storage (Fig 6B), *fatty acid synthase-1* (*fasn1*) (Smith *et al.*, 2003) and *lsd2* (an antagonist of lipases which we have shown to regulate Hh activity, Fig 3) were also significantly upregulated (Fig 6A). Furthermore, Hh staining was found to be more widely distributed in the glial cytoplasm, rather than restricted to the ring-like structures surrounding LDs upon FGF activation (Fig 6C–G, evaluated by the ratio of glial cytoplasm that contains Hh staining).

We next assessed the role of Hh signalling downstream of glial FGF activation. Hh knockdown (RNAi efficiency tested in (Tian *et al.*, 2015)) rescued NB S phase delay (Fig 6H) without affecting glial niche size (Fig EV5A and B). In addition, we used a *LexA/LexAop* binary expression system in conjunction with the *GAL4/UAS* system, to simultaneously activate glial FGF and inhibit NB Hh signalling. Induction of RNAi against *ci* in the NB caused a significant increase in EdU incorporation (Fig 6I, *dnab-GAL4 > ci* RNAi). Together with glial FGF activation, Ci knockdown also significantly rescued NB EdU index (Fig 6I). Together, our results suggest that Hh mediates glia-NB crosstalk downstream of glial FGF activation.

Lipid metabolism genes lie downstream of glial FGF-NB crosstalk

As we previously showed that Lsd-2 modulates Hh activity (Fig 3), we hypothesise that lipid metabolism enzymes function upstream of Hh to regulate NB behaviour. Consistent with this, we found induction of *hh* RNAi upon cortex glial FGF activation did not alter the

number of LDs (Fig EV5C and D). We next explored whether lipid metabolism genes mediate the effects of glial FGF activation on NB proliferation. Glial expression of RNAs targeting lipogenesis genes *fasn1* and *lsd2* efficiently reduced LDs (Fig EV5E–G), but were not required for wild-type NB S phase progression (Fig EV5H). However, knockdown of *Fasn1* and *Lsd2* significantly rescued NB S phase progression defects caused by *htl^{ACT}* overexpression (Figs 6J and Fig EV5I), suggesting lipid metabolism genes function downstream of glial FGF–NB crosstalk.

Fasn1 and Rasp affect glial Hh palmitoylation to regulate NB cell cycle

Hh is known to be synthesised as a precursor protein (HhN) which undergoes a series of post-translational modifications within the secretory pathway (Fig 7A) (Mann & Beachy, 2004). The N- and

C-termini of Hh proteins are covalently modified with palmitate and cholesterol, respectively (Porter *et al*, 1996; Pepinsky *et al*, 1998). Palmitate is a 16-carbon saturated fatty acid, which can either be diet-derived or synthesised via de novo fatty acid synthesis, mediated by enzymes such as *Fasn* and *ACC* (Schiller & Bensch, 1971; Slakey *et al*, 1979; Innis, 2016). Given *Fasn1*, an enzyme involved in de novo synthesis of palmitate, is also involved in glial FGF–NB crosstalk, we assessed whether Hh palmitoylation is required downstream of glial FGF signalling. Palmitoylation of the N-terminal of HhN is mediated by a dedicated acyltransferase in the ER called *Rasp* in *Drosophila* (Fig 7A). In the embryo, *Rasp* has been shown to be required for Hh diffusion (Chamoun *et al*, 2001; Lee & Treisman, 2001; Micchelli *et al*, 2002). We found cortex glial knockdown of *Rasp* whilst not required for NB S phase progression (Fig 7B) was sufficient to rescue NB EdU incorporation defects caused by FGF activation (Fig 7B, *NP2222-GAL4 > htl^{ACT}*).

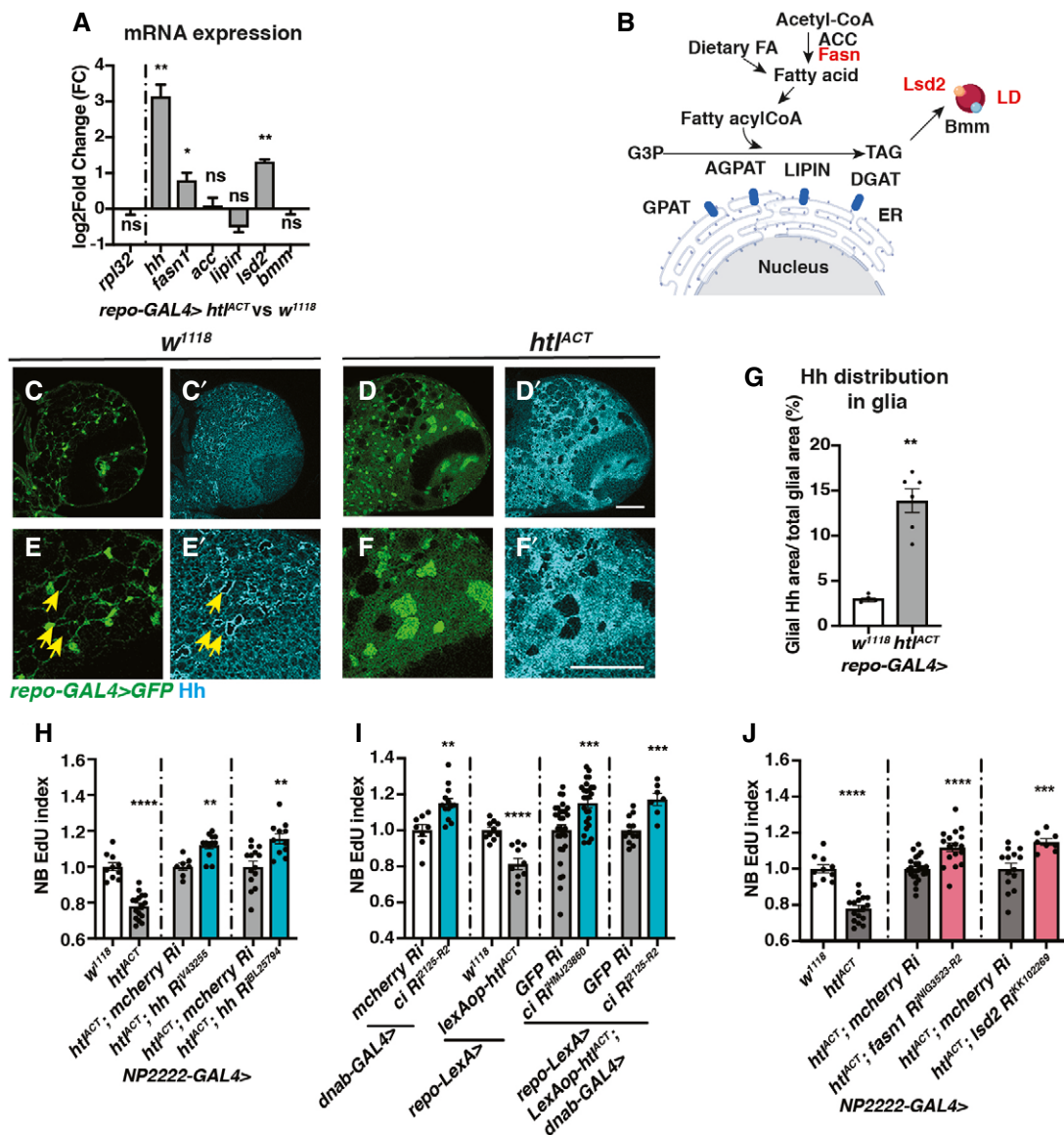


Figure 6.

Figure 6. Hh and lipid metabolism regulators mediate the effects of glial *htl^{ACT}* on NB proliferation.

- A Pan-glial (*repo-GAL4*) *htl^{ACT}* overexpression causes upregulation of *hh*, *fasn1* and *lsd2* transcripts ($n = 3$ biological replicates pooled from 20 brains for each genotype; for each biological replicate, we ran three technical replicates for each PCR reaction). The lipogenesis genes (*acc*, *lipin*), and lipolysis gene *bmm* transcripts are not significantly altered. We utilised *rpl32* as a reference gene in these experiments, as it is not altered by *htl^{ACT}* overexpression. The data are represented by log₂-fold change relative to the control (*repo-GAL4* > *w¹¹¹⁸*).
- B Schematic depicting lipogenesis and lipolysis. Lipogenesis begins with *de novo* synthesis of fatty acids by carboxylation of cytosolic acetyl-CoA via acetyl-CoA carboxylase (ACC) and elongation of fatty chain via fatty acid synthase (Fasn, red). Dietary-derived and *de novo*-generated fatty acids are converted into fatty acylCoA, which re-localises to ER and participates in triglyceride (TAG) synthesis with glycerol-3 phosphate (G3P). This process is mediated by a series of enzymes: glycerol-3-phosphate acyltransferase (GPAT), acylCoA acylglycerol-3-phosphate acyltransferases (AGPAT), Lipin (a phosphatidate phosphatase) and diacylglycerol acyltransferase (DGAT, red). TAG is translocated from the ER to the core of the intracellular organelles called LDs. On the surface of LDs, a triglyceride lipase called Brummer (Bmm), and its inhibitor Lsd-2, antagonistically control TAG storage.
- C–G Representative images showing that Hh staining normally localised to a ring-like structure (yellow arrows), becomes delocalised to the glial cytoplasm upon *htl^{ACT}* overexpression, quantified in (E) ($n = 4, 6$ brain lobes). Glial cells are marked with *repo-GAL4* > *GFP*. (E–F) are zoomed in images of (C–D).
- H Cortex glial (*NP2222-GAL4*>) overexpression of two independent *hh* RNAs significantly rescue EdU incorporation defects caused by *htl^{ACT}* overexpression ($n = 10, 16; 7, 12; 14, 11$ brain lobes). The *NP2222-GAL4* > *w¹¹¹⁸* versus *htl^{ACT}* columns depict the same data as those in Fig 5E.
- I Knockdown of NB Hh signalling pathway (*dnab-GAL4* > *UAS-ciRNAi*) rescues NB EdU incorporation defects induced by glial *htl^{ACT}* overexpression (*repo-LexA* > *LexAop-htl^{ACT}*). Induction of *ciRNAi* in NBs alone increases NB EdU incorporation ($n = 8, 13; 10, 10; 30, 26; 12, 7$ brain lobes).
- J The NB EdU incorporation defects due to cortex glial (*NP2222-GAL4*>) overexpression of *htl^{ACT}* is significantly rescued by overexpression of RNAs against *fasn1* and *lsd2*, compared to corresponding control RNAs ($n = 10, 16; 25, 17; 14, 8$ brain lobes). The *NP2222-GAL4* > *w¹¹¹⁸* versus *htl^{ACT}* columns depict the same data as those in Fig 5E. The control column for *htl^{ACT}*; *lsd2* *Ri^{KKI02269}* depicts the same data as the control column for *htl^{ACT}*; *hh* *Ri^{BL25794}* in Fig 6H.

Data information: Scale bar = 50 μ m. Error bar represents SEM. In (A), *t*-test was conducted to compare log transformed fold change: *rpl32*: Welch's *t*-test, (ns) $P = 0.9355$; *hh*: unpaired *t*-test, (***) $P = 0.0061$; *fasn1*: unpaired *t*-test, (*) $P = 0.0242$; *acc*: unpaired *t*-test, (ns) $P = 0.7570$; *lipin*: unpaired *t*-test, (ns) $P = 0.1222$; *lsd2*: unpaired *t*-test, (***) $P = 0.0074$; *bmm*: unpaired *t*-test, (ns) $P = 0.9356$. In (G): Mann–Whitney test, (***) $P = 0.0095$. In (H): unpaired *t*-test, (****) $P < 0.0001$; Mann–Whitney test, (***) $P = 0.0031$; unpaired *t*-test, (***) $P = 0.0012$. In (I): unpaired *t*-test, (***) $P = 0.0019$; unpaired *t*-test, (****) $P < 0.0001$; Mann–Whitney test, (****) $P = 0.0006$; unpaired *t*-test, (****) $P = 0.0003$. In (J): unpaired *t*-test, (****) $P < 0.0001$; unpaired *t*-test, (****) $P < 0.0001$; Welch's *t*-test, (****) $P = 0.0004$. Source data are available online for this figure.

To test whether Hh palmitoylation is required for its ability to signal to NBs, we expressed a GFP tagged and non-cholesterol modifiable form of HhN in cortex glial cells (Wendler *et al*, 2006; Hartman *et al*, 2013). HhN-GFP was mostly localised to puncta in the glial cytoplasm, and some of these puncta made contact with NBs (Fig 7C–C', *NP2222-GAL4*). The number of puncta making contact with NBs was significantly reduced upon knockdown of Rasp (Fig 7E–E' compared to D–D', G), suggesting that palmitoylation is required for HhN transport from glia to NBs. Similar to full-length Hh (Fig 2J and K), glial HhN expression caused a reduction in NB EdU incorporation (Fig 7H), suggesting that palmitoylated Hh is sufficient for glia–NB crosstalk.

Similar to Rasp knockdown, *Fasn1* knockdown caused a reduction in the number of HhN-GFP puncta that made contact with NBs (Fig 7D–G). To test whether *Fasn1* is functionally required to mediate HhN's ability to cause NB S phase progression defects, we knocked down *Fasn1* whilst overexpressed HhN. In this setting, *Fasn1* knockdown rescued EdU incorporation defects caused by HhN expression (Fig 7I). Together, our data suggest that palmitoylation via Rasp and *Fasn1*, in addition to regulation by *Lsd-2*, are required for Hh function in the context of glia–NB crosstalk.

Glial ROS acts in parallel to lipid–Hh signalling to regulate NB proliferation in the FGF-driven glioma model

Lipid metabolism alteration in glia has previously been linked to reactive oxygen species (ROS), where excessive ROS production causes LD accumulation, which in turn triggers neurodegeneration (Bailey *et al*, 2015; Liu *et al*, 2015). Furthermore, ROS upregulation is known to promote glioblastoma progression (Schieber & Chandel, 2014). We therefore tested whether lipid metabolism changes in the FGF-driven glioma model are correlated with ROS levels. Using ROS-inducible *gstD* promoter–*GFP* reporter (Sykietis & Bohmann, 2008), we detected a 5-fold increase in *gstD-GFP* upon FGF

activation in glial cells (Appendix Fig S1A–C). To decipher the effect of ROS manipulation on lipid metabolism, we overexpressed a *Catalase* (Anderson *et al*, 2005) and a *superoxide dismutase 1* (Martin *et al*, 2009) in cortex glial cells where FGF was activated to suppress ROS. And we found the number of LDs, an indicator of lipid metabolism, was not altered upon ROS reduction (Appendix Fig S1D', E', F', and H). These manipulations were however effective in partially rescuing NB EdU incorporation defects caused by glial FGF activation (Appendix Fig S1I) without affecting glial overgrowth (Appendix Fig S1D–G). We conclude that the production of ROS upon FGF activation in the glial niche potentially acts in parallel with lipid–Hh signalling to inhibit NB proliferation.

Collectively, our findings indicate that the expression of Hh in the cortex glia is required for the formation of glial chambers. Moreover, we demonstrate that expression of Hh in the cortex glial niche must be restrained to prevent ectopic Hh signalling in the NBs. We showed that the ability of glial Hh to signal to NBs is modulated by lipid metabolism enzymes *Fasn1* and *Lsd-2*. Upon overgrowth of the cortex glial niche induced by FGF activation, Hh, lipid metabolism regulators as well as ROS are upregulated in the niche, which in turn slow down the NB cell cycle and affect its ability to generate a full repertoire of neurons (Fig 7J).

Discussion

In the mammalian CNS, neuron and glia interactions are complex. Astrocytes that are structurally related to the cortex glia in *Drosophila* enwrap multiple neurons and NSCs, and are known to modulate adult neurogenesis through soluble signals such as morphogens and extracellular matrix proteins (Spampinato *et al*, 2019). Similarly, the *Drosophila* cortex glial niche, which form chambers that encapsulate NB and its progeny, creates microenvironments that are required for NB maintenance and neuronal maturation (Dumstrei

et al, 2003; Peraanu et al, 2005; Coutinho-Budd et al, 2017; Speder & Brand, 2018; Yuan et al, 2020). Furthermore, glial overgrowth observed in the context of glioblastoma has recently been shown to affect NBs and neuronal survival (Read, 2018; Portela et al, 2019). In this study, we have identified a new mechanism of glia-NB cross-talk via Hh modulated by lipid regulators that affect NB cell cycle progression and lineage size.

During development, NB lineages have been shown to produce its own pool of Hh (Chai et al, 2013), which likely act redundantly with the glial Hh. However, glial Hh levels must be tightly regulated to ensure NB can progress through the cell cycle, and produce the appropriate number and types of neurons. Similar to pro-proliferative

roles of Hh in the astrocytes of the mammalian brain (Ugbo et al, 2017), *Drosophila* glial- Hh is autonomously required for the growth of cortex glial cells and the formation of the glia chambers which surround NBs. Hh knockdown caused NB clustering which in turn induced moderate NB cell cycle delay and reduced neuron production, reminiscent of phenotypes reported for glial PI3K inhibition which also caused disrupted glial chambers (Speder & Brand, 2018). This contrasts with Hh and Smo mutant NB phenotype, previously reported by Chai et al (2013), where they found the loss of NB Hh signalling caused a significant increase in NB clone size. Therefore, our data support the model that glial Hh is required for niche elaboration, which in turn affects NB proliferation.

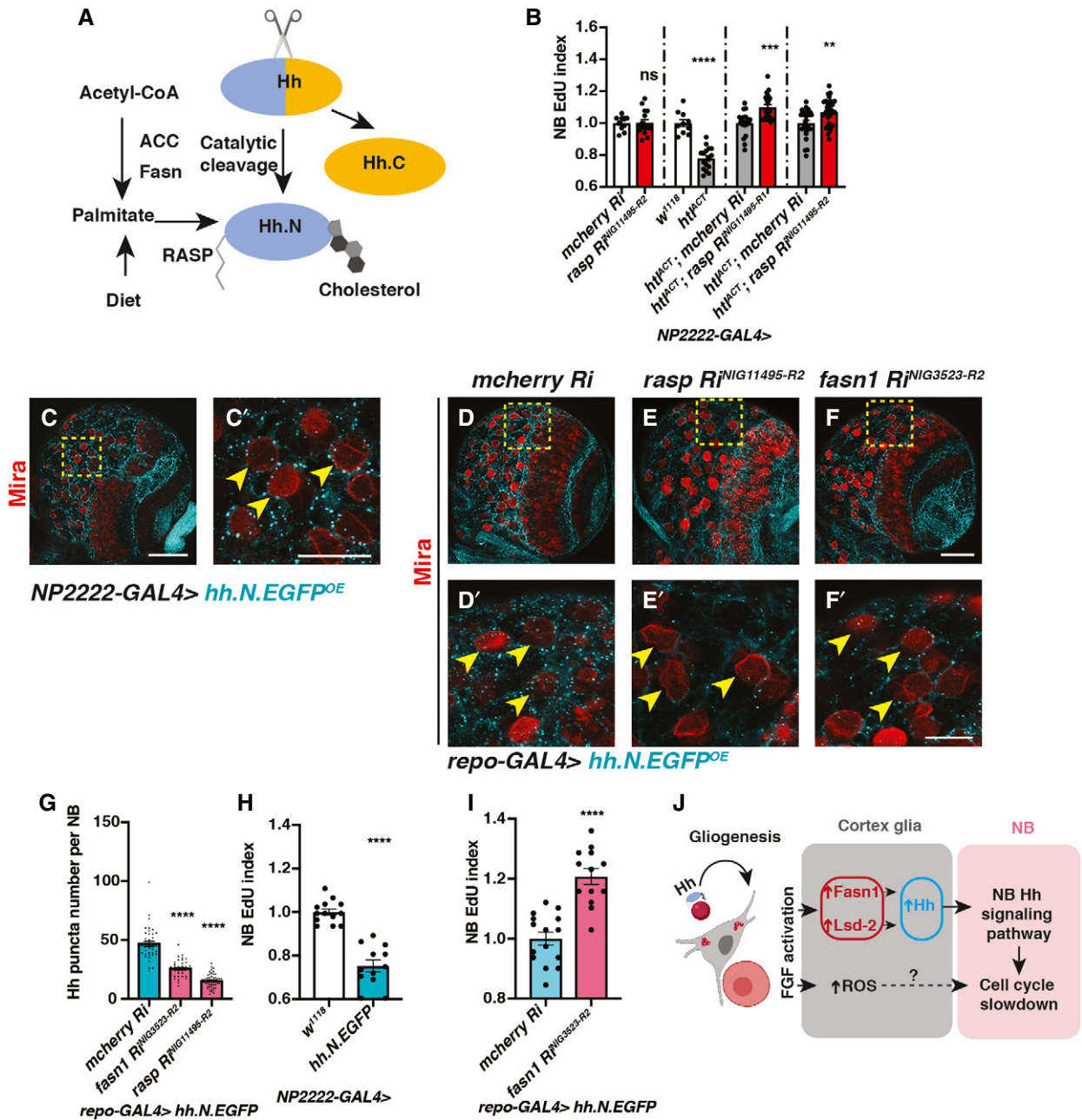


Figure 7.

Figure 7. Fasn1 affects glial Hh palmitoylation to regulate its signalling to NBs.

- A Schematic depicting Hh auto-processing, which starts with the cleavage of the protein into a C-terminal part (Hh.C, yellow) and a N-terminal part (Hh.N, blue), with simultaneous covalent addition of cholesterol. Palmitate, from either diet or *de novo* lipogenesis (via ACC and Fasn), is added onto Hh-N, in a reaction catalysed by an acyltransferase, encoded by *rasp*.
- B Inhibition of palmitoylation (via two independent *rasp RNAi*s) rescues NB EdU incorporation defects induced by cortex glial (*NP2222-GAL4>*) *ht^{ACT}* overexpression, whilst knockdown of *Rasp* in cortex glial cells alone does not alter NB EdU index ($n = 10, 15; 10, 16; 18, 21; 26, 29$ brain lobes). The *NP2222-GAL4 > w¹¹¹⁸* versus *ht^{ACT}* columns depict the same data as those in Fig 5E.
- C–C' Representative images showing that Hh.N.EGFP (which cannot undergo cholesterol modification) are found as puncta on the surface of NBs (yellow arrows) when overexpressed in neighbouring cortex glial cells (*NP2222-GAL4>*).
- D–G Representative images showing that knockdown of *Fasn1* in glial cells (*repo-GAL4>*), where Hh.N.EGFP is overexpressed, significantly reduces the number of Hh.N.EGFP puncta on the surface of NBs (yellow arrows), phenocopying the effect of *Rasp* knockdown, quantified in (G) ($n = 38, 38, 57$ NBs from 4, 4, 8 brain lobes, respectively).
- H Cortex glial (*NP2222-GAL4>*) overexpression of Hh.N.EGFP significantly reduces NB EdU incorporation ($n = 13, 12$ brain lobes).
- I Knockdown of *Fasn1* in glial cells rescues NB EdU incorporation defects, caused by glial Hh.N.EGFP overexpression, quantified in (I) ($n = 15, 13$ brain lobes).
- J Schematic depicting our working model. During development, Hh tethered to LDs are localised to cortex glial cells, to activate gliogenesis. Non-autonomously, excessive glial Hh inhibits NB cell cycle progression. Upon cortex glial-specific FGF activation, increased Hh modified by *Fasn1* and *Lsd-2* together with increased ROS prevent NB proliferation.

Data information: (C, D', E' and F) are zoomed in images of (C, D, E and F), respectively; NBs are marked with Mira. Scale bar = 50 μ m in (C, D, E, F). Scale bar = 20 μ m in (C', D', E' and F). Error bar represents SEM. In (B): unpaired *t*-test, (ns) $P = 0.9403$; unpaired *t*-test, (****) $P < 0.0001$; Mann–Whitney test, (****) $P = 0.0004$; Mann–Whitney test, (**) $P = 0.0047$. In (G): Welch's *t*-test, (****) $P < 0.0001$; Welch's *t*-test, (****) $P < 0.0001$. In (H): unpaired *t*-test, (****) $P < 0.0001$. In (I): unpaired *t*-test, (****) $P < 0.0001$.

Source data are available online for this figure.

Whilst moderate level of Hh is permissive for NB cell cycle progression, excess glial Hh through either its overexpression or via FGF activation also affects NB cell cycle progression and its ability to produce neurons. In this case, excess glial Hh non-autonomously activated Hh signalling in the NBs, which is sensitive to this ligand. Different to other niche-derived secreted molecules, such as Dlp (Kanai *et al*, 2018) and Jeb (Cheng *et al*, 2011), which are necessary but not sufficient to induce changes in the NB, Hh plays a physiologically relevant role in disease models of glial overgrowth caused by FGFR activation. TCGA data show that FGFR1–4 is expressed in different combinations in glioblastoma patient samples, and FGFR1 is an important contributor to poor outcome in glioblastoma (Jimenez-Pascual & Siebzehnrubl, 2019).

In the *Drosophila* brain, cortex glia appears to be the key glial subtype that is responsible for glia-NB crosstalk. Only FGF but not glial InR and EGFR activation caused an expansion of cortex glia (Avet-Rochex *et al*, 2012, 2014), which in turn increased Hh levels and reduced NB proliferation. In cortex glial cells, Hh closely associates with LDs which are analogous to lipoproteins that have been shown to transport Hh for long-range signalling (Panakova *et al*, 2005; Palm *et al*, 2013). Different from lipoproteins, LDs mainly act as lipid storage organelles and are less mobile. Consistent with this, upon FGF activation, genes that promote lipid synthesis

and storage were upregulated. So how does lipid metabolism regulate Hh function? We showed two mechanisms. The first mechanism involves the interaction between lipid storage regulator *Lsd-2* and Hh that colocalise on the surface of LDs and that *Lsd-2* modulates Hh's ability to signal to NBs. It is not yet clear how *Lsd-2* directly regulates Hh activity, but we think it is possible that *Lsd-2* might physically interact with Hh and affect its secretion, or alternatively, *Lsd-2* competes with Hh for positions on the surface of LDs and pushes Hh into the cytoplasm. The second mechanism involves *Fasn1* and *Rasp* which regulates Hh-post-translational modification. Given that lipid synthesis and LDs have recently been reported to be upregulated in glioma, and are emerging as important biomarkers and metabolic targets (Guo *et al*, 2013; Geng & Guo, 2017), it would be interesting to further explore how lipid metabolism regulators affect signalling in this context. In addition to the Hh-LD axis, ROS which is implicated in glioblastoma (Schieber & Chandel, 2014) also lies downstream of FGF-mediated glia-NB crosstalk. Knockdown of both Hh and ROS axes significantly rescued NB cell proliferation defects caused by FGF activation in the glial cells. The phenomenon we reported here together with other reports that glioblastoma affects the survival or proliferation rate of its neighbours (Read, 2018; Portela *et al*, 2019) poses an interesting but yet unexplored prospect that glioma outcompetes NBs within the CNS for limited energy and nutrient resources.

Materials and Methods

Reagents and Tools Table

Reagent/Resource	Reference or Source
Oligonucleotides and other sequence-based reagents	
RT-qPCR primers for <i>rpl32</i>	Akkouche <i>et al</i> (2017)
Forward primer: CCGCTCAAGGGACAGTATCTG	
Reverse primer: ATCTCGCCGAGTAAACGC	

Reagents and Tools table (continued)

Reagent/Resource	Reference or Source
RT-qPCR primers for <i>fasn1</i> Forward primer: TAAGGAGGTCTGCACAAAGCC Reverse primer: CGGTGAGAGGTTGATGATCG	PrimerBlast
RT-qPCR primers for <i>acc</i> Forward primer: CCTCATTAAACCCGCGCTACA Reverse primer: TTTTACGCGCAATGGTGTC	PrimerBlast
RT-qPCR primers for <i>lipin</i> Forward primer: AAACGAAGCTGAGACGGAGAA Reverse primer: GGTTTTGCTCTGGACACCTC	FlyPrimerBank
RT-qPCR primers for <i>lsd2</i> Forward primer: ATTGCCCGTGGTAAATGCC Reverse primer: CGAAGACAGATTTTTGCCTTT	FlyPrimerBank
RT-qPCR primers for <i>bmm</i> Forward primer: GTCTCCTCTGCGATTGGCCAT Reverse primer: CTGAAGGGACCCAGGGAGTA	FlyPrimerBank
RT-qPCR primers for <i>hh</i> Forward primer: TGCTCCGTC AAGTCAGATTCG Reverse primer: GTTGGCGGTCATGCTCAAAA	PrimerBlast

Methods and Protocols

Fly husbandry and strains

Fly stocks were reared on standard *Drosophila* media at 25°C. Crosses for overexpression and knockdown experiment were set up at 25°C, and after a day, the progenies were moved to 29°C, unless otherwise stated.

The fly strains used were as follows: *repo-GAL4* (BDSC7415), *NP2222-GAL4* (KYOTO112830), *wrapper-GAL4* (Coutinho-Budd et al, 2017; Richier et al, 2017), *dnab-GAL4* (From Alex Gould laboratory), *repo-LexA::GAD* (BDSC67096), *w¹¹¹⁸,UAS-htl^{ACT}* (BDSC5367), *UAS-Egfr^{ACT}* (BDSC59843), *UAS-InR^{wt}* (BDSC8262), *LexAop-htl^{ACT}* (generated in this paper), *UAS-GFP*, *UAS-mGFP*, *UAS-dcr2*, *UAS-FUCCI* (BDSC55110), *UAS-lacZ*, *UAS-luc* (BDSC64774) *UAS-hh* (from Thomas B. Kornberg lab), *UAS-hh.N.GFP* (BDSC81023), *UAS-lsd2* (from Alex Gould lab), *UAS-ci^{Ne5m5m(ACT)}* (from Yu Cai lab), *UAS-cat.A* (BDSC24621), *UAS-Sod1.A* (BDSC24754), *UAS-mcherryRNAi* (BDSC35785), *UAS-GFPRNAi* (BDSC9331), *UAS-fasn1RNAis* (NIG3523R-2, NIG3523R-6), *UAS-lsd2RNAis* (VDRC102269, BDSC34617 and BDSC32846), *UAS-hhRNAis* (VDRC43255, BDSC25794), *UAS-ciRNAis* (NIGHMJ23860, NIG2125R-2), *UAS-raspRNAis* (NIG11495R-1, NIG11495R-2), *dpnGFP* (BDSC59755), *his2AV-mRFP* (Kieran Harvey laboratory), Hh:GFP BAC, Ptc:mcherry BAC, *ci-lacZ* (all three lines are generated by Thomas B. Kornberg laboratory), *lsd2YFP* (KYOTO115301) and *gstD-GFP* (From Tatsushi Igaki laboratory), *prosGFP* (VDRC318418). The *repo-MARCM* stock was as follows: *UAS-RedStinger*; *repo-flp*, *repo-GAL4*,

UAS-actinGFP; *FRT82B*, *tub-gal80* (from Joseph M. Bateman laboratory). *w;;FRT82B* was used to generate surface glial clones.

Immunostaining

Larval and pupal brains were dissected in PBS, fixed for 25 min in 4% formaldehyde (Sigma-Aldrich, #F8775) in PBS and rinsed in 0.5% PBST (PBS + 0.5% Triton X-100 (Sigma-Aldrich, #T8787)). For immunostaining, brains were incubated with primary antibodies overnight at 4°C, followed by an overnight secondary antibody incubation at °C. Samples were mounted in 80% glycerol in PBS for image acquisition. The primary antibodies used were mouse anti-Mira (1:50; gift from Alex Gould), rat anti-Mira (1:100, Abcam, #ab197788), rabbit anti-Mira (1:200, gift from Rita Sousa-Nunes), rat anti-pH3 (1:500; Abcam, #ab10543), chick anti-GFP (1:2000; Abcam, #ab13970), rabbit anti-RFP (1:100, Abcam, #ab62341), mouse anti-Fibrillarlin (1:200, Abcam, #ab4566), rabbit anti-Hh (1:500, gift from Isabel Guerrero) and rabbit anti-Insc (1:20, gift from William Chia). Secondary donkey antibodies conjugated to Alexa 555 and Alexa 647 and goat antibody conjugated to Alexa 405, 488, 555 and 647 (Molecular Probes) were used at 1:500. DAPI (Molecular Probes) was used at 1:10,000.

EdU labelling and pulse-chase

EdU *in vitro* labelling was used to identify actively dividing NBs, and larval brains were incubated in 10 μM EdU /PBS for 10–15 min (for 96ALH brains) or 1 h (Fig EV4P–S), followed by fixation, and development using Click-iT Plus EdU Cell Proliferation Kit for imaging, Alexa

Fluor 647 dye (Invitrogen, #C10640), following the manufacturer's instruction. The brain tissues were then stained with Mira to label NBs. Control and experimental brains were processed in the same tube to ensure they were exposed to the same incubation conditions.

EdU pulse-chase was used to identify the progeny of dividing NBs. 3rd instar larvae were fed with instant fly food supplemented with 100 µg/ml EdU (Lee et al, 2006) for 3 h. They were then transferred to standard *Drosophila* media for a 3 or 4 h EdU chase. Wandering stage larvae were collected for brain dissection, followed by fixation, development and immunostaining as described above.

LD staining

For LD staining, larval brains were dissected in PBS, fixed and rinsed in PBS before incubation in HCS LipidTOX Red Neutral Lipid Stain (Invitrogen, #H34476, 1:1,000 in PBS) for 1 h. These samples were then rinsed and mounted in PBS and imaged directly to preserve LD morphology. For experiments that require LD staining together with immunostaining, the tissues were rinsed three times in PBS after immunostaining to remove all PBST and incubated with LD dyes as described above. The tissues were mounted in 80% glycerol in PBS for imaging.

Imaging and image processing

Images were collected on a Leica SP5 or Olympus FV3000 confocal microscopes and analysed using Fiji (<https://imagej.net/Fiji>). Z stacks of CBs were imaged, and the ventral side of the CB was shown as the representative image unless otherwise stated.

Live cell imaging

Dissected brains (72ALH) were cultured in Schneider's culture medium supplemented with 10% inactivated FBS, 2% Penicillin-Streptomycin solution (Sigma-Aldrich, #P4458), 20 µM glutamine and Schneider's culture medium (Gibco, #21720024) and dissected fat body from the same animals. The brains were imaged in a µ-Slide 8 well (Ibidi, #80806) on an Olympus FV3000 microscope using resonance scanner in 16Bit mode, with a 40×/0.95 lens and 2× zoom. Z stacks with 2 µm intervals were captured every 2 min over a period of 3–8 h. Laser intensity was kept low to avoid cytotoxicity. AVI movies were generated using Fiji.

All the images were processed using Adobe Photoshop and compiled using Adobe Illustrator. For the purpose of better presentation, image brightness adjustments were applied equally to controls and experiments.

Quantitative reverse transcription PCR

For gene expression analysis, 20 dissected late 3rd-instar larval brains were lysed in 300 µl TRI Reagent (ZYMO Research, #R2061) to form one biological replica. Three biological replicates were prepared for each genotype: *repo-GAL4 > w¹¹¹⁸* and *repo-GAL4 > htl^{ACT}*. Total RNA was extracted using a Direct-zol RNA Microprep Kit (ZYMO Research, #R2061), and 1 µg of total RNA from each sample was reverse transcribed into cDNA using ProtoScript II First Strand cDNA Synthesis Kit (NEB, #E6560S) according to the manufacturer's instructions. The qPCR was performed using the stepOnePlus real-time PCR system (Applied Biosystems) using Fast SYBR Green master mix reagent (Applied Biosystems, #4385612). Gene expression levels were normalised to *rpl32* (in Fig 6A, one representative data set of *rpl32* was plotted) and calculated using the 2^{-ΔΔCt} method.

The primers were either designed using Primer-BLAST (<https://www.ncbi.nlm.nih.gov/tools/primer-blast/>) or obtained from FlyPrimerBank (<https://www.flyrnai.org/flyprimerbank>).

Listed in Reagents Table.

Molecular cloning

A constitutively active form of *htl*, comprising the dimerisation domain of the bacteriophage λ repressor (Michelson et al, 1998), was amplified from the genomic DNA of the fly stock: *UAS-htl^{ACT}* (BDSC5367), using a forward primer, 5'-CAACTGCAACTACT-GAAATCTGCC-3', and a reverse primer 5'-CCCCCTCTAGATTAA-TAATTACACCACTTCTGC-3'. The resulting PCR product was digested with *NotI* (Promega, #R6431) and *XbaI* (Promega, #R6181), which cut at the restriction sites as indicated in the reverse primer (underlined above). The plasmid, *pJFRC19-13XLexAop2-IVS-myr::GFP* (Addgene, #26224), was identically digested to remove *myr::GFP*. The restriction fragment, *NotI-htl^{ACT}-XbaI*, was subsequently cloned into the digested LexAop vector (Pfeiffer et al, 2010). The reconstructed plasmid was sequenced and injected into flies carrying an attP2 docking site (BDSC25710).

Quantification and analysis

Hh and LipidTOX intensity profile

A flat line was drawn across each LDs as described in Fig 1H, and single pixel values of Hh and LipidTOX staining were generated along line using "Analyze-Plot Profile" tool of Fiji. The intensity profiles of Hh and LipidTOX for each LDs were compiled using Prism-GraphPad, with Y-axis reflecting pixel values and X-axis reflecting relative position on LDs. The relative LD position was generated by dividing the line position values to each line length. This normalisation was conducted because line length is different in each sample due to the variations in LD size. The Hh intensity at the position X_{0.9} (Fig 1H, at the surface of LDs) was compared with that of the position X_{1.0} (Fig 1H, just outside of LDs) to illustrate the Hh-LD association described in Fig 1C–G'.

Cortex glial membrane size, LD volume and glial number measurement

Cortex glial membrane volume (*NP2222-GAL4 > UAS-mGFP*) and LD volume were measured from three-dimensional reconstruction of confocal Z stacks (2-µm step-size) with Volocity software (Improvision). Glial cell number was automatically counted with a Fiji plug-in "DeadEasy Larval Glia" (Forero et al, 2012).

Cell cycle speed

The number of type I NBs in each brain lobe was manually counted using Fiji. type I NBs were distinguished from other Mira⁺ cells by size and morphology: Newly generated GMCs are smaller than type I NBs as shown in Fig EV3E (white arrows). Type II NBs are associated with more Mira⁺ progeny cells.

EdU index: For 26ALH larval brains, EdU voxels of the whole brain were measured with Volocity software (Improvision) to indicate NB re-entry into cell cycle. Glial EdU voxels represents only a small amount of the total EdU voxels (Sousa-Nunes et al, 2011). Normalised EdU voxels were calculated by dividing EdU voxels to the mean voxel counts of the control. For 96ALH larval brains, the number of EdU⁺ type I NBs was counted in the CB of each brain lobe. EdU index is calculated as number of EdU⁺ NBs normalised to control EdU⁺ NBs. The number of EdU⁺ NBs reflects

the NBs that progress through S phase in a 10 or 15-min time window relative to control. We have utilised GAL4 driver > *w¹¹¹⁸*, *UAS-mcherryRNAi* or *UAS-luc* interchangeably as controls in our experiments, as we found EdU incorporation did not significantly alter between these controls (Appendix Fig S2). The total number of type I NBs is not altered in experiments where Edu index was used to determine NB cell cycle speed. For EdU pulse-chase quantification, the number of progeny cells that inherit EdU from each dividing NBs was counted to indicate the speed by which NBs generate their progeny.

pH3 index: represented as the % of type I NBs in M phase ($pH3^+$) / the total number of type I NBs.

Cell cycle lengths in NBs were measured as the time between two consecutive cell divisions. The cell cycle lengths of NBs from at least three different ex vivo brains were plotted for each genotype.

CNS and cell size measurement

Brain lobes, NB, GMC and nucleoli diameters were estimated by averaging orthogonal measurements of diameter, with a single confocal section on Fiji. The volume of each brain lobe (CNS) was calculated by the formula: $V = 4/3\pi r^3$.

Localisation of asymmetric determinants was assessed in M phase NBs that display a condensed metaphase plate marked by pH3. Clear crescent localisation was counted as correct localisation, and cytoplasmic or cortical localisation was counted as mislocalisation.

The distribution of Hh in glia was measured on Fiji with the formula: The area of glia that contains Hh / Total glial area. The detailed procedure: Total glial area: Adjust Threshold (Default) > Analysis > measure (area); The area of glia that contains Hh: Create selection of glial channel by Adjusting Threshold (Default) > Restore selection in the Hh channel > clear outside > measure area.

Total intensity

The sum projection confocal image was used for the intensity measurement on Fiji using the formula: CTCF (corrected total cell fluorescence) = Integrated density – (Area of selected cell x mean fluorescence of background readings) (McCloy et al, 2014).

Statistical analysis

P-values were calculated by two-tailed, unpaired Student's *t*-test, with equal sample variance; Welch's correction was applied in case of unequal variances. Kolmogorov–Smirnov test was used to test data normality. Mann–Whitney test was used when data deviated from a normal distribution. Data are presented as mean ± SEM in the main text.

Data availability

This study includes no data deposited in external repositories.

Expanded View for this article is available online.

Acknowledgements

We are grateful to Alex Gould, Thomas B. Kornberg, Isabel Guerrero, Yu Cai, William Chia, Tatsushi Igaki, Joseph M. Bateman, Kieran Harvey, Helena Richardson, Gary Hime and Philip Batterham for generous sharing of

antibodies and fly stocks. We would like to thank Bloomington Drosophila Stock Center, Vienna Drosophila Resource Center, Fly Stocks of National Institute of Genetics, KYOTO Stock Center, Developmental Studies Hybridoma Bank and Addgene for fly stocks and plasmids. We would like to also thank OZDros for *Drosophila* quarantine, Peter MacCallum Cancer Institute Microscopy core and Biological Optical Microscopy platform at the University of Melbourne for technical assistance. We would like to thank Charles Robin and Mike Murray for sharing their microinjection facility with us. We are grateful to Kieran Harvey, Helena Richardson and Andrew Cox for critical reading of the manuscript. Schematic pictures in the figures are created with BioRender. QD is funded by a Melbourne Research Scholarship, LYC is funded by an ARC Future Fellowship, and LYC's laboratory is supported by funding from the NHMRC, ARC and the Peter MacCallum Cancer Foundation.

Author contributions

QD, MZ, FF, TL and SG conducted the experiments; QD and LYC designed the experiments and wrote the paper.

Conflict of interest

The authors declare that they have no conflict of interest.

References

- Akkouche A, Mugat B, Barckmann B, Varela-Chavez C, Li B, Raffel R, Pelisson A, Chambeyron S (2017) Piwi Is Required during *Drosophila* embryogenesis to license dual-strand piRNA clusters for transposon repression in adult ovaries. *Mol Cell* 66: 411–419 e414
- Anderson PR, Kirby K, Hilliker AJ, Phillips JP (2005) RNAi-mediated suppression of the mitochondrial iron chaperone, frataxin, in *Drosophila*. *Hum Mol Genet* 14: 3397–3405
- Avet-Rochex A, Kaul AK, Gatt AP, McNeill H, Bateman JM (2012) Concerted control of gliogenesis by InR/TOR and FGF signalling in the *Drosophila* post-embryonic brain. *Development* 139: 2763–2772
- Avet-Rochex A, Maierbrugger KT, Bateman JM (2014) Glial enriched gene expression profiling identifies novel factors regulating the proliferation of specific glial subtypes in the *Drosophila* brain. *Gene Expr Patterns* 16: 61–68
- Awasaki T, Lai SL, Ito K, Lee T (2008) Organization and postembryonic development of glial cells in the adult central brain of *Drosophila*. *J Neurosci* 28: 13742–13753
- Bailey AP, Koster G, Guillermier C, Hirst EM, MacRae JI, Lechene CP, Postle AD, Gould AP (2015) Antioxidant role for lipid droplets in a stem cell niche of *Drosophila*. *Cell* 163: 340–353
- Chai PC, Liu Z, Chia W, Cai Y (2013) Hedgehog signaling acts with the temporal cascade to promote neuroblast cell cycle exit. *PLoS Biol* 11: e1001494
- Chamoun Z, Mann RK, Nellen D, von Kessler DP, Bellotto M, Beachy PA, Basler K (2001) Skinny Hedgehog, an acyltransferase required for palmitoylation and activity of the Hedgehog signal. *Science* 293: 2080–2084
- Chandra V, Das T, Gulati P, Biswas NK, Rote S, Chatterjee U, Ghosh SN, Deb S, Saha SK, Chowdhury AK et al (2015) Hedgehog signaling pathway is active in GBM with GLI1 mRNA expression showing a single continuous distribution rather than discrete high/low clusters. *PLoS One* 10: e0116390
- Chell JM, Brand AH (2010) Nutrition-responsive glia control exit of neural stem cells from quiescence. *Cell* 143: 1161–1173

- Chen W, Huang H, Hatori R, Kornberg TB (2017) Essential basal cytonemes take up Hedgehog in the *Drosophila* wing imaginal disc. *Development* 144: 3134–3144
- Cheng LY, Bailey AP, Leever SJ, Ragan TJ, Driscoll PC, Gould AP (2011) Anaplastic lymphoma kinase spares organ growth during nutrient restriction in *Drosophila*. *Cell* 146: 435–447
- Coutinho-Budd JC, Sheehan AE, Freeman MR (2017) The secreted neurotrophin Spatzle 3 promotes glial morphogenesis and supports neuronal survival and function. *Genes Dev* 31: 2023–2038
- Dienstmann R, Rodon J, Prat A, Perez-Garcia J, Adamo B, Felip E, Cortes J, lafrate AJ, Nuciforo P, Taberner J (2014) Genomic aberrations in the FGFR pathway: opportunities for targeted therapies in solid tumors. *Ann Oncol* 25: 552–563
- Ding WY, Huang J, Wang H (2020) Waking up quiescent neural stem cells: molecular mechanisms and implications in neurodevelopmental disorders. *PLoS Genet* 16: e1008653
- Doe CQ (1996) Spindle orientation and asymmetric localization in *Drosophila*: both inscuteable? *Cell* 86: 695–697
- Doe CQ (2017) Temporal patterning in the *Drosophila* CNS. *Annu Rev Cell Dev Biol* 33: 219–240
- Doyle SE, Pahl MC, Siller KH, Ardifff L, Siegrist SE (2017) Neuroblast niche position is controlled by phosphoinositide 3-kinase-dependent DE-cadherin adhesion. *Development* 144: 820–829
- Dumstrei K, Wang F, Hartenstein V (2003) Role of DE-cadherin in neuroblast proliferation, neural morphogenesis, and axon tract formation in *Drosophila* larval brain development. *J Neurosci* 23: 3325–3335
- Forero MG, Kato K, Hidalgo A (2012) Automatic cell counting in vivo in the larval nervous system of *Drosophila*. *J Microsc* 246: 202–212
- Freeman MR (2015) *Drosophila* central nervous system glia. *Cold Spring Harb Perspect Biol* 7: a020552
- Geng F, Guo D (2017) Lipid droplets, potential biomarker and metabolic target in glioblastoma. *Intern Med Rev* 3: <https://doi.org/10.18103/imr.v3i5.443>
- Guo D, Bell EH, Chakravarti A (2013) Lipid metabolism emerges as a promising target for malignant glioma therapy. *CNS Oncol* 2: 289–299
- Hartman TR, Strohlic TI, Ji Y, Zinshteyn D, O'Reilly AM (2013) Diet controls *Drosophila* follicle stem cell proliferation via Hedgehog sequestration and release. *J Cell Biol* 201: 741–757
- Hayashi S, Ito K, Sado Y, Taniguchi M, Akimoto A, Takeuchi H, Aigaki T, Matsuzaki F, Nakagoshi H, Tanimura T et al (2002) GETDB, a database compiling expression patterns and molecular locations of a collection of Gal4 enhancer traps. *Genesis* 34: 58–61
- Heemskerk J, DiNardo S (1994) *Drosophila* Hedgehog acts as a morphogen in cellular patterning. *Cell* 76: 449–460
- Homem CC, Knoblich JA (2012) *Drosophila* neuroblasts: a model for stem cell biology. *Development* 139: 4297–4310
- Hoyle G (1986) Glial cells of an insect ganglion. *J Comp Neurol* 246: 85–103
- Hoyle G, Williams M, Phillips C (1986) Functional morphology of insect neuronal cell-surface/glial contacts: the trophospongium. *J Comp Neurol* 246: 113–128
- Innis SM (2016) Palmitic acid in early human development. *Crit Rev Food Sci Nutr* 56: 1952–1959
- Jimenez-Pascual A, Siebzehrnubi FA (2019) Fibroblast growth factor receptor functions in glioblastoma. *Cells* 8: 715
- Kanai MI, Kim MJ, Akiyama T, Takemura M, Wharton K, O'Connor MB, Nakato H (2018) Regulation of neuroblast proliferation by surface glia in the *Drosophila* larval brain. *Sci Rep* 8: 3730
- Kis V, Barti B, Lippai M, Sass M (2015) Specialized cortex glial cells accumulate lipid droplets in *Drosophila melanogaster*. *PLoS One* 10: e0131250
- Lai SL, Lee T (2006) Genetic mosaic with dual binary transcriptional systems in *Drosophila*. *Nat Neurosci* 9: 703–709
- Lee JD, Treisman JE (2001) Sightless has homology to transmembrane acyltransferases and is required to generate active Hedgehog protein. *Curr Biol* 11: 1147–1152
- Lee CY, Wilkinson BD, Siegrist SE, Wharton RP, Doe CQ (2006) Brat is a Miranda cargo protein that promotes neuronal differentiation and inhibits neuroblast self-renewal. *Dev Cell* 10: 441–449
- Liu L, Zhang K, Sandoval H, Yamamoto S, Jaiswal M, Sanz E, Li Z, Hui J, Graham BH, Quintana A et al (2015) Glial lipid droplets and ROS induced by mitochondrial defects promote neurodegeneration. *Cell* 160: 177–190
- Mann RK, Beachy PA (2004) Novel lipid modifications of secreted protein signals. *Annu Rev Biochem* 73: 891–923
- Martin I, Jones MA, Grotewiel M (2009) Manipulation of Sod1 expression ubiquitously, but not in the nervous system or muscle, impacts age-related parameters in *Drosophila*. *FEBS Lett* 583: 2308–2314
- Maurange C, Cheng L, Gould AP (2008) Temporal transcription factors and their targets schedule the end of neural proliferation in *Drosophila*. *Cell* 133: 891–902
- McCloy RA, Rogers S, Caldon CE, Lorca T, Castro A, Burgess A (2014) Partial inhibition of Cdk1 in G2 phase overrides the SAC and decouples mitotic events. *Cell Cycle* 13: 1400–1412
- Micchelli CA, The I, Selva E, Mogila V, Perrimon N (2002) Rasp, a putative transmembrane acyltransferase, is required for Hedgehog signaling. *Development* 129: 843–851
- Michelson AM, Gisselbrecht S, Buff E, Skeath JB (1998) Heartbroken is a specific downstream mediator of FGF receptor signalling in *Drosophila*. *Development* 125: 4379–4389
- Morrison RS, Yamaguchi F, Saya H, Bruner JM, Yahanda AM, Donehower LA, Berger M (1994) Basic fibroblast growth factor and fibroblast growth factor receptor I are implicated in the growth of human astrocytomas. *J Neurooncol* 18: 207–216
- Nusslein-Volhard C, Wieschaus E (1980) Mutations affecting segment number and polarity in *Drosophila*. *Nature* 287: 795–801
- Palm W, Swierczynska MM, Kumari V, Ehrhart-Bornstein M, Bornstein SR, Eaton S (2013) Secretion and signaling activities of lipoprotein-associated Hedgehog and non-sterol-modified Hedgehog in flies and mammals. *PLoS Biol* 11: e1001505
- Panakova D, Sprong H, Marois E, Thiele C, Eaton S (2005) Lipoprotein particles are required for Hedgehog and wingless signalling. *Nature* 435: 58–65
- Pepinsky RB, Zeng C, Wen D, Rayhorn P, Baker DP, Williams KP, Bixler SA, Ambrose CM, Garber EA, Miatkowski K et al (1998) Identification of a palmitic acid-modified form of human sonic Hedgehog. *J Biol Chem* 273: 14037–14045
- Pereanu W, Shy D, Hartenstein V (2005) Morphogenesis and proliferation of the larval brain glia in *Drosophila*. *Dev Biol* 283: 191–203
- Pfeiffer BD, Ngo TT, Hibbard KL, Murphy C, Jenett A, Truman JW, Rubin GM (2010) Refinement of tools for targeted gene expression in *Drosophila*. *Genetics* 186: 735–755
- Portela M, Venkataramani V, Fahey-Lozano N, Seco E, Losada-Perez M, Winkler F, Casas-Tinto S (2019) Glioblastoma cells vampirize WNT from neurons and trigger a JNK/MMP signaling loop that enhances glioblastoma progression and neurodegeneration. *PLoS Biol* 17: e3000545
- Porter JA, Young KE, Beachy PA (1996) Cholesterol modification of Hedgehog signaling proteins in animal development. *Science* 274: 255–259

- Ramon-Canellas P, Peterson HP, Morante J (2019) From early to late neurogenesis: neural progenitors and the glial niche from a fly's point of view. *Neuroscience* 399: 39–52
- Read RD, Cavenee WK, Furnari FB, Thomas JB (2009) A *Drosophila* model for EGFR-Ras and PI3K-dependent human glioma. *PLoS Genet* 5: e1000374
- Read RD (2018) Pvr receptor tyrosine kinase signaling promotes post-embryonic morphogenesis, and survival of glia and neural progenitor cells in *Drosophila*. *Development* 145: dev164285
- Reddy BV, Irvine KD (2011) Regulation of *Drosophila* glial cell proliferation by Merlin-Hippo signaling. *Development* 138: 5201–5212
- Richier B, Vijandi CM, Mackensen S, Salecker I (2017) Lapsyn controls branch extension and positioning of astrocyte-like glia in the *Drosophila* optic lobe. *Nat Commun* 8: 317
- Scadden DT (2014) Nice neighborhood: emerging concepts of the stem cell niche. *Cell* 157: 41–50
- Schieber M, Chandel NS (2014) ROS function in redox signaling and oxidative stress. *Curr Biol* 24: R453–R462
- Schiller H, Bensch K (1971) De novo fatty acid synthesis and elongation of fatty acids by subcellular fractions of lung. *J Lipid Res* 12: 248–255
- Schwartz C, Locke J, Nishida C, Kornberg TB (1995) Analysis of cubitus interruptus regulation in *Drosophila* embryos and imaginal disks. *Development* 121: 1625–1635
- Shen CP, Jan LY, Jan YN (1997) Miranda is required for the asymmetric localization of Prospero during mitosis in *Drosophila*. *Cell* 90: 449–458
- Slakey LL, Ferrick TJ, Ness GC, Porter JW (1979) De novo fatty acid synthesis and fatty acid elongation catalyzed by subcellular fractions from hog and human aorta. *Lipids* 14: 451–457
- Smith S, Witkowski A, Joshi AK (2003) Structural and functional organization of the animal fatty acid synthase. *Prog Lipid Res* 42: 289–317
- Sousa-Nunes R, Yee LL, Gould AP (2011) Fat cells reactivate quiescent neuroblasts via TOR and glial insulin relays in *Drosophila*. *Nature* 471: 508–512
- Spampinato SF, Bortolotto V, Canonico PL, Sortino MA, Grilli M (2019) Astrocyte-derived paracrine signals: relevance for neurogenic niche regulation and blood-brain barrier integrity. *Front Pharmacol* 10: 1346
- Speder P, Brand AH (2018) Systemic and local cues drive neural stem cell niche remodelling during neurogenesis in *Drosophila*. *eLife* 7: e30413
- Sykiotis GP, Bohmann D (2008) Keap1/Nrf2 signaling regulates oxidative stress tolerance and lifespan in *Drosophila*. *Dev Cell* 14: 76–85
- Takezaki T, Hide T, Takanaga H, Nakamura H, Kuratsu J, Kondo T (2011) Essential role of the Hedgehog signaling pathway in human glioma-initiating cells. *Cancer Sci* 102: 1306–1312
- Teixeira L, Rabouille C, Rorth P, Ephrussi A, Vanzo NF (2003) *Drosophila* Perilipin/ADRP homologue Lsd2 regulates lipid metabolism. *Mech Dev* 120: 1071–1081
- Tian A, Shi Q, Jiang A, Li S, Wang B, Jiang J (2015) Injury-stimulated Hedgehog signaling promotes regenerative proliferation of *Drosophila* intestinal stem cells. *J Cell Biol* 208: 807–819
- Ugbode CI, Smith I, Whalley BJ, Hirst WD, Rattray M (2017) Sonic Hedgehog signalling mediates astrocyte crosstalk with neurons to confer neuroprotection. *J Neurochem* 142: 429–443
- Varjosalo M, Taipale J (2008) Hedgehog: functions and mechanisms. *Genes Dev* 22: 2454–2472
- Wendler F, Franch-Marro X, Vincent JP (2006) How does cholesterol affect the way Hedgehog works? *Development* 133: 3055–3061
- Witte HT, Jeibmann A, Klambt C, Paulus W (2009) Modeling glioma growth and invasion in *Drosophila melanogaster*. *Neoplasia* 11: 882–888
- Yamada SM, Yamaguchi F, Brown R, Berger MS, Morrison RS (1999) Suppression of glioblastoma cell growth following antisense oligonucleotide-mediated inhibition of fibroblast growth factor receptor expression. *Glia* 28: 66–76
- Yuan X, Sipe CW, Suzawa M, Bland ML, Siegrist SE (2020) Dilp-2-mediated PI3-kinase activation coordinates reactivation of quiescent neuroblasts with growth of their glial stem cell niche. *PLoS Biol* 18: e3000721
- Zielke N, Korzelius J, van Straaten M, Bender K, Schuhknecht GFP, Dutta D, Xiang J, Edgar BA (2014) Fly-FUCCI: a versatile tool for studying cell proliferation in complex tissues. *Cell Rep* 7: 588–598